Origin of ultramafic–mafic bodies on the Isles of Lewis and Harris (Scotland, UK): constraints on the Archean–Paleoproterozoic evolution of the Lewisian Gneiss Complex, North Atlantic Craton

George L. Guice[1], Sophie R. Miocevich[2], Hannah S. R. Hughes[3], Iain McDonald[4], Kathryn M. Goodenough[5]; Michael R. Ackerson[1]; John M. MacDonald[6]; John W. Faithfull[7]

[1] Department of Mineral Sciences, National Museum of Natural History, Smithsonian Institution, 10th Street & Constitution Avenue, Washington, D.C. 20560, USA

[2] Department of Earth Sciences, University of Cambridge, Downing Street, Cambridge, CB2 3EQ, UK

[3] Camborne School of Mines, College of Engineering, Mathematics & Physical Sciences, University of Exeter, Penryn Campus, Penryn, Cornwall, TR10 9FE, UK

[4] School of Earth and Ocean Sciences, Cardiff University, Main Building, Park Place, Cardiff. CF10 3AT, UK

[5] British Geological Survey, The Lyell Centre, Research Avenue South, Edinburgh EH14 4AP, UK

[6] School of Geographical and Earth Sciences, University of Glasgow, Glasgow G12 8QQ, UK

[7] Hunterian Museum, University of Glasgow, University Avenue, Glasgow, G12 8QQ, UK

*corresponding author: GuiceG@si.edu

Keywords: Platinum-group elements; PGE; Metaperidotite; Metapyroxenite; Cratonization; Scourie Dykes; Archean tectonics.

ABSTRACT

The Lewisian Gneiss Complex (LGC) is a tonalite-trondhjemite-granodiorite (TTG)-dominated fragment of the North Atlantic Craton (NAC) in northwest Scotland. End-member models describe the LGC as representing either a continuous piece of Archean crust or up to 12 geologically distinct Archean terranes, with interpretations sitting on a spectrum between these end-members. There is particular uncertainty over the correlations between the Archean–Paleoproterozoic magmatic and metamorphic events recorded by mainland part of the LGC and the part exposed on the Outer Hebridean islands of Lewis and Harris. In this paper, we present the results of field mapping, petrography, and major, trace and platinum-group element (PGE) bulk-rock geochemistry for four ultramafic–mafic bodies in Lewis and Harris, namely: Maaruig, Loch Mhorsgail, Coltraiseal Mor and Beinn a' Chuailean. We consider the effects of metamorphism and element mobility, their petrogenesis, and potential correlations with ultramafic–mafic rocks elsewhere in the LGC. Our data indicate that the studied ultramafic–mafic rocks can be subdivided into two petrologically distinct groups. Metaperidotites and metapyroxenites from Maaruig and Loch Mhorsgail are interpreted as Archean (> 2.8 Ga) cumulates distinct from anything currently identified in the mainland LGC, with this interpretation based on distinctive modal layering, a discordance with surrounding TTG gneiss, fractionated PGE patterns ($[Pd/Ir]_N$ = 1.3–6.6) and negative HFSE anomalies ($[Nb/La]_N$ = 0.2–0.8). Metagabbronorites from Coltraiseal Mor and Beinn a' Chuailean, which also exhibit negative high field strength-element (HFSE) anomalies ($[Nb/La]_N$ = 0.2–0.7) and show mildly fractionated ($[Pd/Ir]_N$ = 1.2–2.8) PGE patterns, most likely represent deformed Paleoproterozoic dykes. These occurrences could be correlatives of a suite of ca. 2.4 Ga mafic dykes exposed throughout the mainland LGC (the Scourie Dykes), with the Outer Hebridean occurrences having experienced more intense Paleoproterozoic (Laxfordian) deformation/reworking. These interpretations suggest that the LGC lithologies of Lewis and Harris were proximal to the mainland LGC's Central Region by the early Paleoproterozoic but raises the possibility that they were distinct crustal blocks in the Mesoarchean.

1.0 INTRODUCTION

The Lewisian Gneiss Complex (LGC) in northwest Scotland (Fig. 1a) is a fragment of tonalite-trondhjemite-granodiorite (TTG) Archean crust variably reworked during the Proterozoic (e.g., Wheeler et al., 2010). The Archean–Paleoproterozoic evolution of the LGC is described by competing models, including end-member interpretations whereby it is interpreted to represent: (a) a section of broadly continuous Archean crust that has been subsequently faulted to expose different crustal levels (Park and Tarney, 1987); or (b) up to 12 geologically unique terranes that assembled later, during the Proterozoic (Kinny et al., 2005 and references therein).

This regional debate, whereby interpretations sit on a spectrum between the two end-member models outlined above, reflects a broader discussion about the nature of Archean geodynamics and the onset of plate tectonics (e.g., Kamber, 2015). While many envisage plate tectonics to have commenced by the late Archean (ca. 2.8 Ga; de Wit et al., 1987; Furnes et al., 2007; Dhuime et al., 2015; Brown and Johnson, 2018; Cawood et al., 2018), others argue that key plate tectonic indicators (e.g., blueschists and ophiolites) are absent in the Archean and rare in the Proterozoic, with this geodynamic regime therefore not predominating on Earth until the Neoproterozoic (ca. 1.0–0.85 Ga; Hamilton, 2003; Stern, 2005, 2008, 2020). Fundamentally, was Archean continental crust — such as that preserved in the LGC — formed and assembled by processes akin to modern-style plate tectonics, or was an alternative geodynamic regime, such as stagnant-lid tectonics, responsible (Bédard, 2013; Debaille et al., 2013; Stern, 2016)?

Much of the previous research on this topic in the LGC has focused on felsic lithologies (Kinny and Friend, 1997; Friend and Kinny, 2001; Love et al., 2010; Whitehouse and Kemp, 2010; MacDonald et al., 2013), with a smaller body of work considering the mafic rocks (e.g,. Sills et al., 1982; Johnson et al., 2012; Guice et al., 2020; Fischer et al., 2021). In this paper, we focus on ultramafic–mafic lithologies, whose origin(s) can potentially be attributed to a wide-range of magmatic settings that have varied potential implications for broad-scale geodynamic processes predominant on Earth. For

example, the preservation of fragments of oceanic lithosphere — as suggested for a plethora of Archean–Proterozoic ultramafic complexes globally (Kusky et al., 2001, 2007; Anhaeusser, 2006; Furnes et al., 2007; Dilek and Polat, 2008; Ordóñez-calderón et al., 2009; Kisters and Szilas, 2012; Szilas et al., 2013; Grosch and Slama, 2017) — requires a different suite of magmatic and tectonic processes to that of komatiites or associated layered intrusions. In the latter case, the ultramafic rocks would have crystallized from a magma derived from high degrees of partial melting and became juxtaposed with the TTG gneiss, possibly via. "sagduction" (e.g., Johnson et al., 2016).

The temporal and petrogenetic relationship between ultramafic–mafic magmatism exposed in the Scottish mainland (see Guice et al., 2020 and references therein) and Outer Hebridean portions of the LGC also remains unresolved (Fettes and Mendum, 1987; Mason and Brewer, 2004). Some authors have correlated the Archean–Paleoproterozoic rocks in the Outer Hebrides with those in mainland Scotland (Fettes and Mendum, 1987), while others argue — in-line with the terrane model described above — that they comprise several distinctive crustal blocks that amalgamated during the late Paleoproterozoic (Kinny et al., 2005). In the latter scenario, the Outer Hebrides Fault Zone (OHFZ), which is a north-northeast/south-southwest-trending structure that can be traced for 170 km along the east coast of the Outer Hebridean islands of Barra, South Uist, Benbecula, North Uist and Lewis and Harris (Fig. 1a; Jehu and Craig, 1924, 1927, 1934; Cheadle et al., 1987; Imber et al., 1997), could be a late Paleoproterozoic (ca. 1.6 Ga) suture (Friend and Kinny, 2001; Mason and Brewer, 2004; Kinny et al., 2005; Love et al., 2010; Mason, 2016).

In this paper, we focus on four Outer Hebridean ultramafic–mafic bodies whose age(s) and origin(s) are enigmatic, namely Maaruig, Loch Mhorsgail, Coltraiseal Mor and Beinn a' Chuailean (Fig. 1b). For these localities, we present the results of field mapping and observations, petrography, and major, trace and platinum-group element (PGE) bulk-rock geochemistry. Using these data, we aim to: (a) establish age relations with the surrounding TTG gneiss; (b) consider the effects of metamorphism and element mobility; (c) discuss the likely origin(s) of the ultramafic–mafic bodies; (d) test the possible

97 correlations with ultramafic–mafic magmatism exposed in the mainland LGC; and (e) consider any

98 implications for the Archean–Paleoproterozoic evolution of the LGC.

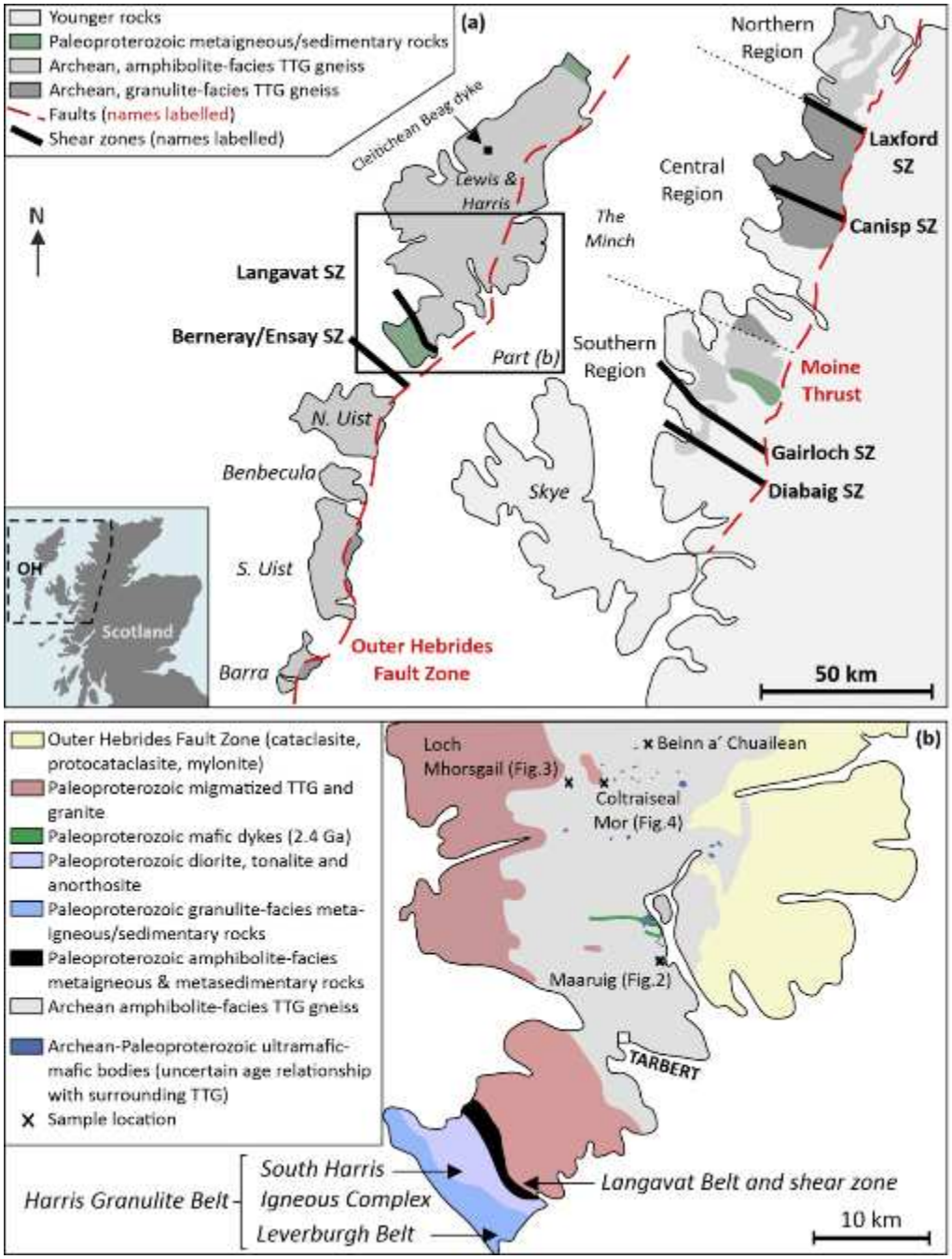

99

100 **Figure 1: (a)** Simplified geological map of the Lewisian Gneiss Complex, NW Scotland (redrawn after: Wheeler et al., 2010;

101 MacDonald and Goodenough, 2013). Abbreviations: SZ = shear zone; TTG = tonalite-trondhjemite-granodiorite. **(b)**

102 Geological map of the island of south Lewis and Harris, which is the focus of this study (redrawn after: Fettes et al., 1992).

103 The area represented is highlighted in part (a).

2.0 GEOLOGICAL FRAMEWORK

The Archean–Paleoproterozoic LGC is a small fragment of the NAC that crops out on the Outer Hebrides and the northwest Scottish mainland (Fig. 1a). The LGC predominantly comprises Archean, amphibolite- to granulite-facies TTG gneiss, with minor ultramafic, mafic and metasedimentary lithologies (Peach et al., 1907; Sutton and Watson, 1951; Fettes and Mendum, 1987; Wheeler et al., 2010). These lithologies, which have been subject to multiple phases of amphibolite–granulite-facies metamorphism, are cross-cut by Paleoproterozoic mafic dykes (ca. 2.4–2.0 Ga; Teall 1885, Mason and Brewer 2004, Davies and Heaman 2014) and Paleo- to Meso-proterozoic granitic–pegmatitic intrusions (Dearnley, 1962; Davies et al., 1975; Fettes and Mendum, 1987; Park et al., 2002; Shaw et al., 2016). Paleoproterozoic (ca. 2.2–1.9 Ga) belts comprising metasedimentary and meta-igneous lithologies are also a minor component of the LGC; both in the mainland (e.g., Loch Maree Group; Floyd et al. 1989) and Outer Hebrides (e.g., Harris Granulite Belt; Langavat Belt; Whitehouse and Bridgwater 2001, Mason et al. 2004a, 2004b, Hollis et al. 2006, Mason 2016).

2.1 The Lewisian Gneiss Complex of mainland Scotland

Cropping out as a 125 km long, 20 km wide coastal strip (Fig. 1a), the mainland LGC is traditionally subdivided into a granulite-facies Central Region and amphibolite-facies Northern and Southern Regions (e.g., Wheeler et al. 2010 and references therein). The pyroxene-bearing gneisses of the Central Region have been previously interpreted as representing deeper crustal levels than the hornblende-bearing gneisses of the Northern and Southern Regions (Park and Tarney, 1987). Geochronological studies — generally involving U-Pb dating of zircon from the TTG gneisses — have revealed a geographically diverse suite of protolith and metamorphic ages for these lithologies (Kinny and Friend, 1997; Friend and Kinny, 2001; Love et al., 2004, 2010; Kinny et al., 2005). One interpretation of these data, which represents the alternate end-member to the traditional subdivision described above, is that the mainland LGC comprises six distinct “terranes” that have unique Archean histories and were tectonically juxtaposed during the Proterozoic (e.g., Kinny et al.

2005). Although the number, extent and significance of individual terranes remains a matter for discussion (e.g., Fischer et al., 2021), the Laxford and Gairloch Shear Zones (Fig. 1a) are generally accepted as major crustal boundaries (Park, 2005; Goodenough et al., 2010, 2013).

A broad magmatic and metamorphic chronology is relatively well constrained for the Central Region of the mainland LGC (Fig. 2). The igneous protoliths of the TTG gneisses crystallized between 3.1 and 2.7 Ga (Kinny and Friend, 1997; Friend and Kinny, 2001; Love et al., 2004; Whitehouse and Kemp, 2010; MacDonald et al., 2013, 2015). This was followed by a granulite–amphibolite-facies tectonothermal episode between 2.7 and 2.5 Ga (Taylor et al., 2020), whereby the lower crust could have been at high temperature and melt-bearing for more than 200 m.y.. This protracted tectonothermal episode has also been interpreted as two discrete metamorphic events (e.g., Fischer et al. 2021 and references therein): known locally as the granulite-facies Badcallian (ca. 2.7 Ga; Evans and Lambert, 1974; Barnicoat, 1983; Cartwright et al., 1985; Corfu et al., 1994; Andersen et al., 1997; Corfu, 1998; Barooah and Bowes, 2009; Crowley et al., 2015; Feisel et al., 2018) and granulite- to amphibolite-facies Inverian (ca. 2.5 Ga Beach, 1973, 1974; Corfu et al., 1994; Whitehouse and Kemp, 2010). The Badcallian–Inverian structures are cross-cut by a suite of mafic dykes, largely emplaced 2.42–2.38 Ga, which are known locally as the Scourie Dykes (Teall, 1885; Peach et al., 1907; Sutton and Watson, 1951; Davies and Heaman, 2014; Hughes et al., 2014). Dyke emplacement was followed by multiple greenschist- to amphibolite-facies metamorphic events in the late Paleoproterozoic (ca. 1.9–1.6 Ga) — collectively referred to as the Laxfordian (Beach, 1974; Beach et al., 1974; Goodenough et al., 2010, 2013).

2.1.1 Archean ultramafic, mafic and metasedimentary rocks in the mainland LGC

Ultramafic–mafic complexes occur throughout the granulite-facies Central Region, ranging from cm-scale pods to km-scale complexes (O'Hara, 1961; Bowes et al., 1964, 1966; Davies, 1974; Rollinson and Windley, 1980; Sills et al., 1982; Rollinson and Gravestock, 2012; Johnson et al., 2016; Guice et al., 2018a, 2018b, 2020). The relative proportions of the ultramafic and mafic rocks vary dramatically between individual complexes, with some containing no ultramafic rocks and others comprising

almost entirely these lithologies (Guice, 2019). With some exceptions, the ultramafic portions are generally metapyroxenite-dominated, form the stratigraphic base of individual occurrences and display primary magmatic layering (Sills, 1981; Sills et al., 1982; Guice et al., 2018a, 2020). The mafic portions of these complexes are predominantly mesocratic- to melanocratic (rarely leucocratic), comprise variable portions of garnet, plagioclase, orthopyroxene, clinopyroxene and amphibole (Johnson et al., 2012, 2016), and sometimes preserve relict magmatic layering (Sills, 1981; Sills et al., 1982; Guice et al., 2018a, 2020). Some of these occurrences — notably in the Laxford Shear Zone (Fig. 1a), are spatially associated with quartz-feldspar-biotite-(garnet) gneisses that could be interpreted as metamorphosed sedimentary or volcanogenic lithologies (Beach et al., 1974; Cartwright et al., 1985; Goodenough et al., 2010, 2013; Johnson et al., 2016).

These ultramafic–mafic complexes have previously been the subject of wide-ranging interpretations, including their formation as: (1) the remnants of an early (possibly oceanic) crust that pre-dates the TTG protoliths (Sills, 1981); (2) fragments of one or more layered intrusions (Bowes et al., 1964; Guice et al., 2018a, 2020); (3) accreted oceanic crust (Park and Tarney, 1987); (4) fragments of Archean mantle (Guice et al., 2020); or (5) sagducted remnants of one or more greenstone belt(s) (Johnson et al., 2016). Recent studies have suggested that these lithologies may reflect more than one origin (Rollinson and Gravestock, 2012; Johnson et al., 2016; Guice et al., 2018a, 2020), and possibly record multiple phases of temporally distinct ultramafic–mafic magmatism (Guice et al., 2020).

Based on field mapping, petrographic characteristics, and bulk-rock major, trace and platinum group element geochemistry, Guice et al. (2020) subdivided these mainland Archean ultramafic–mafic complexes into two groups: (1) a large group of distinctly layered bodies, interpreted as representing ca. 2.8 Ga layered intrusions; and (2) a smaller group of peridotite-rich bodies that are generally massive (weakly layered in places), likely pre-date the TTG and record a more enigmatic, possibly mantle origin. Unlike the layered ultramafic–mafic bodies, which display consistent concordance between TTG gneissosity, lithological contacts and layering in the ultramafic–mafic rocks, the second

group of ultramafic bodies occur as discordant, elliptical-shaped pods dominated by metaperidotite (Faithfull et al., 2018; Guice et al., 2020). Note that this "layered" vs. generally massive "peridotitic" distinction is made for the Archean ultramafic–mafic complexes in the mainland LGC throughout this paper (Fig. 2).

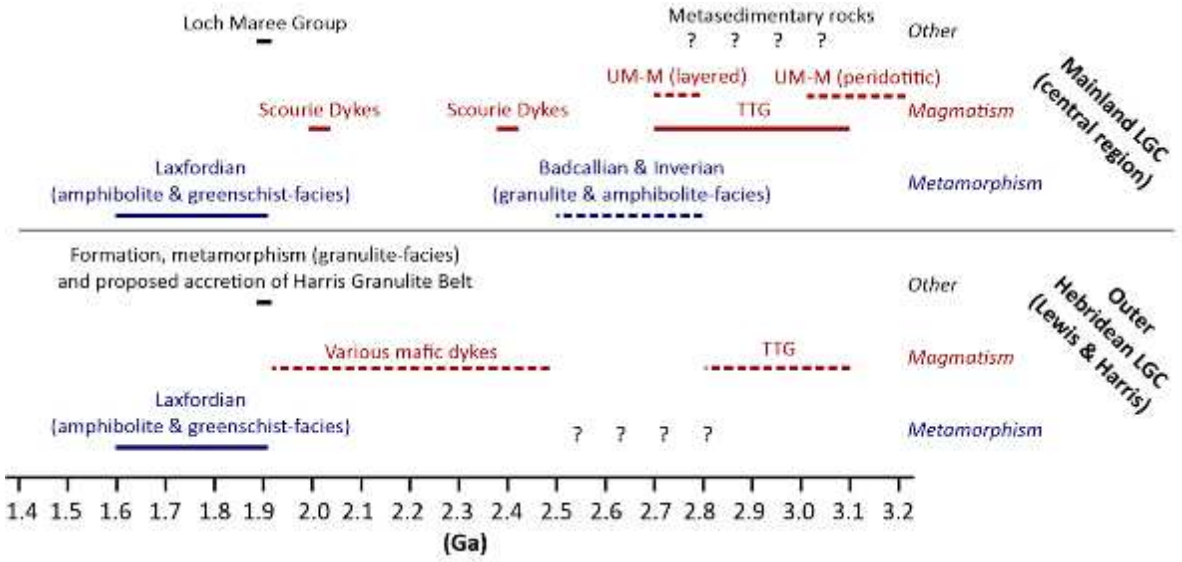

Figure 2: Timeline detailing the major magmatic and metamorphic events currently recognized the mainland (Central Region) and Outer Hebridean (Lewis and Harris; often referred to as the Tarbert Terrane) portions of the LGC. Dashed lines represent moderate uncertainty. Question marks represent high uncertainty. See text for references.

2.1.2 Paleoproterozoic Scourie Dykes in the mainland LGC

The Scourie Dykes are a suite of steeply-dipping northwest/southeast to east/west-trending mafic dykes that mostly intruded between 2.42 and 2.38 Ga (Davies and Heaman, 2014), with a smaller group of ca. 2.0 Ga occurrences also identified (Heaman and Tarney, 1989). Individual dykes are up to 100 m wide, display sharp contacts with the surrounding TTG and, although they are most widespread in the Central Region, exist in all 3 regions of the mainland LGC (Sutton and Watson, 1951; Weaver and Tarney, 1981). Based on the primary mineral assemblages, the Scourie Dykes of the Central Region (Fig. 1) can be subdivided into several groups (Tarney, 1963; Weaver and Tarney, 1981; Tarney and Weaver, 1987; Hughes et al., 2014): (1) a texturally and mineralogically homogenous dolerite suite — comprising 90–95 % of the total dykes exposed in the mainland LGC — that is composed of amphibolitized clinopyroxene, plagioclase, hornblende, quartz and biotite, with accessory magnetite,

ilmenite, pyrite, pyrrhotite and apatite; (2) a picrite suite, containing olivine, orthopyroxene and clinopyroxene phenocrysts, alongside interstitial plagioclase, minor phlogopite, and accessory chromite, magnetite, ilmenite and pyrite; and (3) an olivine gabbro suite, comprising orthopyroxene, clinopyroxene, olivine, plagioclase, hornblende and minor phlogopite, alongside accessory magnetite, ilmenite, pyrite and pyrrhotite.

The restriction of the most Mg-rich dykes (the picrite suite) to the Central Region has been used to suggest that these magmas did not ascend to the mid-crustal levels represented by the Northern and Southern Regions (Hughes et al., 2014). As has been documented for multiple extension-related Paleoproterozoic dykes swarms globally (e.g., Sandeman and Ryan, 2008; Stepanova and Stepanov, 2010), the Scourie Dykes display negative high field strength element (HFSE) anomalies, alongside enrichments in the large ion lithophile elements (LILE: e.g., Th and the light rare earth elements; Hughes et al., 2014). Modelling by Hughes et al. (2014) suggested that this geochemical signature reflects partial melting of sub-continental lithospheric mantle (SCLM), which had been metasomatized either during shallow-angle subduction in the NAC or by carbonatite-induced metasomatism (Yaxley et al., 1991).

2.2 The Lewisian Gneiss Complex of the Outer Hebrides

The OHFZ separates the LGC of the Outer Hebrides into “eastern gneisses” and “western gneisses” (Dearnley, 1962; Fig. 1). The eastern gneisses, which have been most intensely deformed in north Lewis, are often correlated with the mainland LGC, with rocks in southeast Barra preserving evidence for granulite-facies “Badcallian” (see Section 2.1) metamorphism at 2.73 Ga (Fettes and Mendum, 1987; Kinny et al., 2005; MacDonald and Goodenough, 2013). Proposed correlations between the Archean–Paleoproterozoic geology of the western gneisses and the mainland LGC (e.g., Dearnley 1962, Fettes and Mendum 1987) are more controversial, with some authors interpreting the OHFZ as representing a key suture in the Paleoproterozoic amalgamation of the LGC (e.g., Imber et al. 2002, Kinny et al. 2005).

West of the OHFZ, the LGC of Lewis and Harris (often referred to as the "Tarbert Terrane") predominantly comprises ca. 3.1–2.8 Ga, amphibolite-facies TTG gneiss (Jehu and Craig 1927, 1934, Dearnley 1962, Soldin 1978, Fettes and Mendum 1987, Friend and Kinny 2001, Mason et al. 2004a), with these rocks cross-cut by mafic (Paleoproterozoic) dykes (Mason and Brewer 2004, Davies and Heaman 2014). These lithologies are pervasively affected by a late Paleoproterozoic (1.9–1.6 Ga) amphibolite-facies metamorphic event correlated with the Laxfordian of the mainland LGC (see Section 2.1; Fig. 2) that resulted in local migmatization of the TTG gneiss and the intrusion of granites and pegmatites (Dearnley, 1962; Davies et al., 1975; Shaw et al., 2016). Also present are late Archean to mid-Paleoproterozoic metasedimentary and metaigneous lithologies. This includes the Harris Granulite Belt and Langavat Belt in south Harris (Dearnley 1963, Cliff et al. 1983, Baba 1998, 1999, Whitehouse and Bridgwater 2001, Mason et al. 2004a, Hollis et al. 2006, Kelly et al. 2008, Mason 2016), and the Ness Assemblage in northernmost Lewis (Coward et al., 1969; Watson, 1969; Whitehouse, 1990).

The Harris Granulite Belt (Fig. 1b) is composed of two broadly defined components: (1) the Leverburgh Belt, which predominantly comprises psammitic and pelitic metasedimentary rocks, alongside minor mafic rocks, ultramafic rocks, chert and marble; and (2) the South Harris Igneous Complex, which is dominated by tonalite, metagabbro and anorthosite, with minor ultramafic rocks and trondhjemite pegmatites (Dearnley, 1963). The Harris Granulite Belt experienced 1.9 Ga, granulite-facies metamorphism ($T \geq 900^{\circ}$, $P \leq 12.5$ kbar; Baba 1998, 1999, Hollis et al. 2006) not experienced by the TTG gneiss of Lewis and Harris, and is interpreted as an accreted island arc terrane (Whitehouse and Bridgwater 2001, Mason et al. 2004b).

The Langavat Belt, which separates the South Harris Igneous Complex from the TTG gneisses (Fig. 1b), contains highly deformed felsic orthogneiss and metasedimentary rocks, alongside minor mafic and ultramafic rocks, and pelitic metasedimentary rocks. Although its precise origin is enigmatic (Mason et al. 2004a), the Langavat Belt is related to the emplacement of the Harris Granulite Belt (Kelly et al.

2008; Mason 2012). It has not experienced granulite-facies metamorphism, with Archean zircons from the metasedimentary rocks suggesting that they could have been derived from the TTG gneisses to the north (Mason et al. 2004a).

2.2.1 Ultramafic–mafic rocks in Lewis and north Harris

The ultramafic–mafic rocks in Lewis and Harris appear as < 0.5 km^2, variably deformed/dismembered lenses and remnants within both the TTG gneiss and Langavat Belt (Dearnley, 1962, 1963; Dearnley and Dunning, 1967; Myers and Lisle, 1971; Cliff et al., 1998; Mason and Brewer, 2004). Some occurrences cross-cut the gneissose foliation of the surrounding TTG, while others display concordance with this fabric and have more uncertain age relationships (Dearnley and Dunning, 1967; Mason and Brewer, 2004). Based on the preserved mineral assemblages, textures and grain sizes, these ultramafic–mafic bodies have been subdivided into two groups (Dearnley, 1962; Myers and Lisle, 1971): (1) mafic rocks — comprising < 0.5 cm diameter clinopyroxene and hornblende "clots" surrounded by a plagioclase-dominated groundmass — that show relatively uniform textures and no evidence for layering or chilled margins; and (2) coarse-grained, commonly layered ultramafic–mafic rocks, comprising olivine, orthopyroxene, clinopyroxene, plagioclase and hornblende in variable proportions, alongside minor chromite and phlogopite. The latter, relatively coarse-grained and more ultramafic group are less common, but are distinctive in the field, typically displaying light brown weathered surfaces (Dearnley, 1962; Myers and Lisle, 1971).

Several authors have considered all of the ultramafic–mafic rocks to represent deformed mafic dykes that can likely be correlated with the Scourie Dykes of the mainland LGC (Dearnley, 1962; Myers and Lisle, 1971; Davies et al., 1975; Fettes and Mendum, 1987; Cliff and Rex, 1989). This hypothesis is supported by comparable relict igneous textures and by the age of one ultramafic–mafic body on the island of Lewis — the Cleitichean Beag Dyke — which has been dated at 2.41 Ga using U-Pb zircon geochronology (Davies and Heaman, 2014). In this scenario, the general preservation of ultramafic–mafic rocks as small, < 0.5 km^2 remnants would reflect the variable deformational effects of the

Laxfordian metamorphic event. Moreover, the ultramafic occurrences could represent co-magmatic plutonic complexes that intruded deeper crustal levels than the predominantly mafic Scourie Dykes (Dearnley, 1962).

More recent studies have shown that the ultramafic–mafic bodies may record more than one magmatic event. Based on U-Pb zircon geochronology, some of the ultramafic–mafic bodies in Harris (north of the Langavat shear zone and south of Tarbert; Fig. 1b) have been suggested to be a suite of mid-Paleoproterozoic mafic dykes (Mason and Brewer, 2004). It has been speculated that this represents a period of extension — prior to the accretion of the ca. 1.9 Ga Harris Granulite Belt — that could be correlated with the ca. 2.05 Ga Kangamiut dykes in the Greenlandic portion of the NAC (Mason and Brewer, 2004). It has also been suggested that some of the concordant and more ultramafic bodies may represent another group of ultramafic–mafic bodies that could be older than the TTG gneiss (Mason and Brewer, 2004).

3.0 MAPPING AND FIELD RELATIONSHIPS

Three ultramafic–mafic bodies were mapped and subject to detailed field observations and sampling, namely: Maaruig (Section 3.1); Loch Mhorsgail (Section 3.2); and Coltraiseal Mor (Section 3.3). A fourth locality — Beinn a' Chuailean — was also subject to field observations and sampling (see Section 4.0), but was not mapped due to its comparably small size, limited outcrop, and time constraints during fieldwork. It should also be noted that the "meta" prefix is applied to all rock names used throughout this paper, as all four ultramafic–mafic bodies have been subject to amphibolite-facies metamorphism and associated hydrothermal alteration.

3.1 Maaruig

The Maaruig Complex (Myers and Lisle, 1971) forms an elliptical-shaped, 0.6 km x 0.5 km body comprising metapyroxenite and metaperidotite, with localized metre-scale occurrences of metaolivine-gabbro (Fig. 3a). The ultramafic rocks are extremely prominent, forming distinctive brown

outcrops that stand proud of the relatively flat and poorly-exposed surrounding TTG gneiss. Our mapping subdivides the Maaruig Complex into the following units: metapyroxenite (with minor metaperidotite) displaying prominent, mm- to cm-scale orthopyroxene grains; metapyroxenite (with minor metaperidotite) without the prominent orthopyroxene; and honeycomb-weathered metaperidotite that sometimes contains mm- to cm-scale pyroxene oikocrysts (containing olivine and spinel-group mineral chadocrysts). All units commonly contain mm-scale phlogopite. The contacts between metapyroxenite without prominent orthopyroxene and other units are generally sharp, whilst the contacts between metapyroxenite with prominent orthopyroxene and metaperidotite vary from sharp to gradational on the meter-scale. Decimetre-scale, east-west-trending layering can be traced across the mapped area, which is consistent with cm-scale layering observed in individual outcrops (Fig. 3b). The orthopyroxene-bearing metapyroxenite exhibits dark grey to brown weathered surfaces, with 5–40 mm diameter orthopyroxenes which are weathering-resistant relative to the groundmass (Fig. 3c-d). Metaperidotite displays brown weathered surfaces and honeycomb weathering, with individual voids generally 5–10 cm in diameter (Fig. 3e). The orthopyroxene-poor metapyroxenite, which exhibits dark grey weathered surfaces, comprises 1–2 mm diameter olivine and pyroxene grains.

The TTG gneiss displays a mm-scale gneissose foliation that exhibits generally moderate dips and is defined by variation in the modal abundance of quartz, feldspar and amphibole (minor mica is also present). The contacts between the ultramafic rocks and surrounding TTG gneiss are obscured by vegetation, with no outcrop-scale, cross-cutting relationships observed. The gneissose foliation in the TTG is consistently parallel to the margins of the ultramafic-mafic complex, but there is some discordance between the map-scale layering, outcrop-scale layering and complex margins, most notably in the northeast of the mapped area (Fig. 3a). Rare plagioclase is noted in the ultramafic rocks close to some contacts with TTG gneiss, with this feature best observed on the foreshore in the northeast of the mapped area (Fig. 3a).

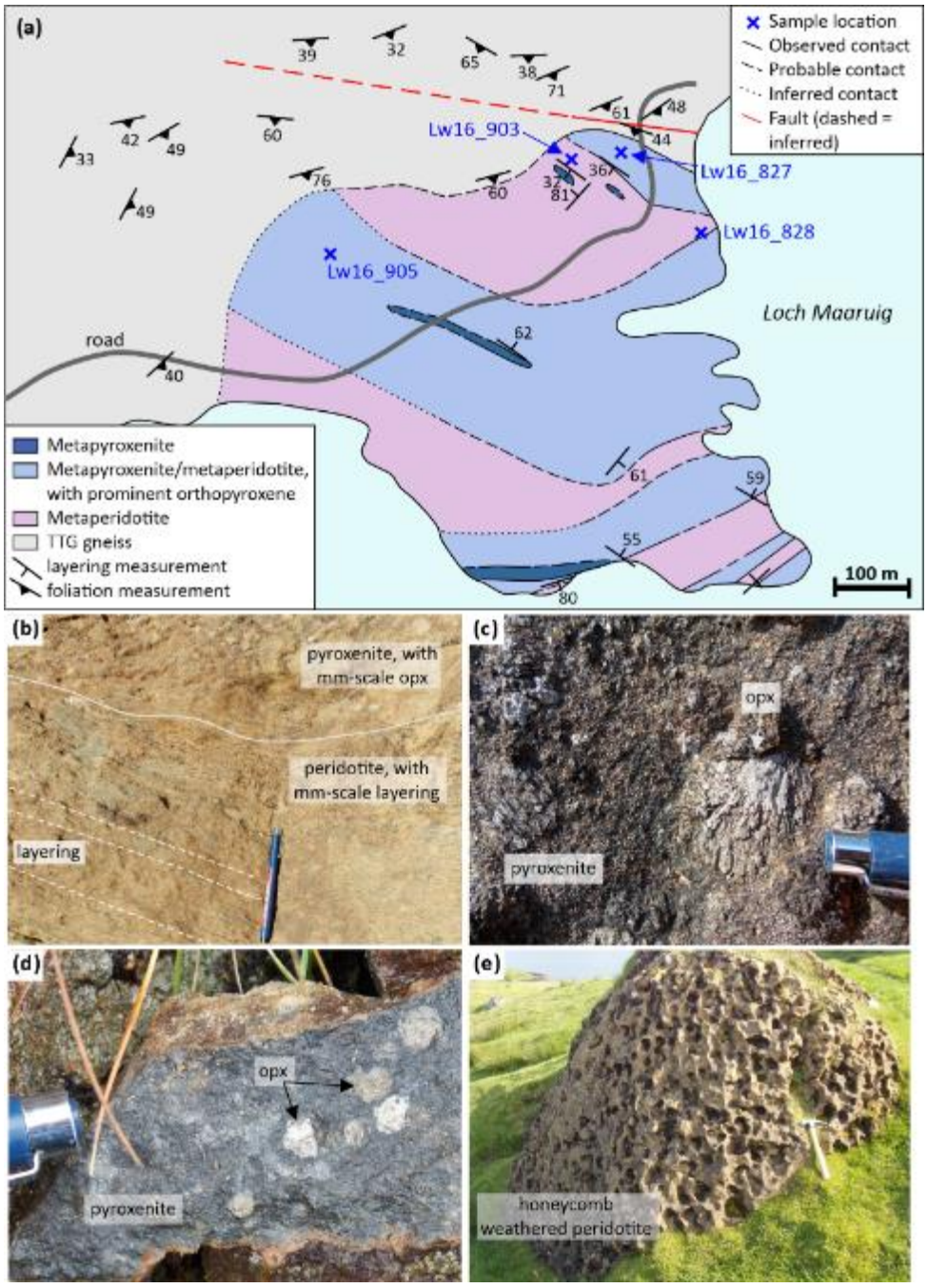

Figure 3: (a) Geological map of the Maaruig Complex. See Fig. 1b for its location in southern Lewis. **(b-e)** Field photographs detailing the typical field relationships displayed by the ultramafic rocks. Hammer length = 33 cm; pen length = 13.5 cm.

3.2 Loch Mhorsgail

The ultramafic rocks of the Loch Mhorsgail Complex — exposed over an area of < 0.5 km^2 and described here for the first time — occur as small (generally meter- to decimeter-scale), low-lying

outcrops located on the shore and islands of Loch Mhorsgail, with minor outcrops inland to the NW of Loch Mhorsgail (Fig. 4a–b). Contacts with the surrounding TTG gneiss are not exposed, but the gneissose foliation in the TTG is generally parallel to the layering in the ultramafic rocks where exposed (Fig. 4a–b). Despite this, there exists some map-scale discordance between the layering and gneissose foliation (specifically on the NE shore of the loch; Fig. 4a–b), but the nature of these contacts (i.e., whether they are tectonic or primary) is unclear. Given both this and the relatively poor exposure, the lateral continuity of the ultramafic rocks is uncertain, with two possible interpretations presented in Figure 4.

The Loch Mhorsgail Complex contains both metapyroxenite (dark-grey weathered surfaces) and metaperidotite (brown weathered surfaces), with individual outcrops exhibiting modal layering that is also defined by the diameter of orthopyroxene grains (Fig. 4c–f). Boundaries between individual layers range from sharp to gradational (over 5–10 cm), with an outcrop-scale example detailed in Figure 4c. Metapyroxenite, which exhibits dark grey to brown weathered surfaces, contains prominent 0.5–4.0 cm diameter orthopyroxene grains alongside rare, mm-scale phlogopite grains. Metaperidotite, which commonly displays honeycomb-weathered textures similar to those at Maaruig (Fig. 3e), also contains prominent, mm-to cm-scale orthopyroxene and rare phlogopite.

The TTG gneiss is composed of feldspar, quartz, amphibole and biotite in varied proportions, with amphibole and mica commonly comprising > 30 % of the mineral assemblage observed in hand specimen. The gneissose foliation, which occurs on the mm-scale and reveals cm- to m-scale isoclinal folds in places, generally displays moderate to steep dips towards the east that are broadly parallel with the trend of the ultramafic–mafic body (Fig. 4). TTG gneiss outcrops also commonly exhibit cm- to m-scale mafic layers/pods, with their spatial distribution detailed in Figure 4. Such layers, which are consistently wrapped by the TTG foliation, predominantly comprise amphibole and plagioclase, with garnet preserved in the centre of larger occurrences. Restricted to the TTG, quartz-feldspar pegmatites occur on the cm- to m-scale, and exhibit grain-sizes ranging from 3–10 cm diameter. The

355 pegmatites occur with increasing frequency/size with increasing proximity to the ultramafic–TTG
356 contact and contain cm scale biotite mica within ~ 10m of the contact. Moreover, these pegmatites
357 are generally concordant with the TTG foliation, but locally cross-cut it.

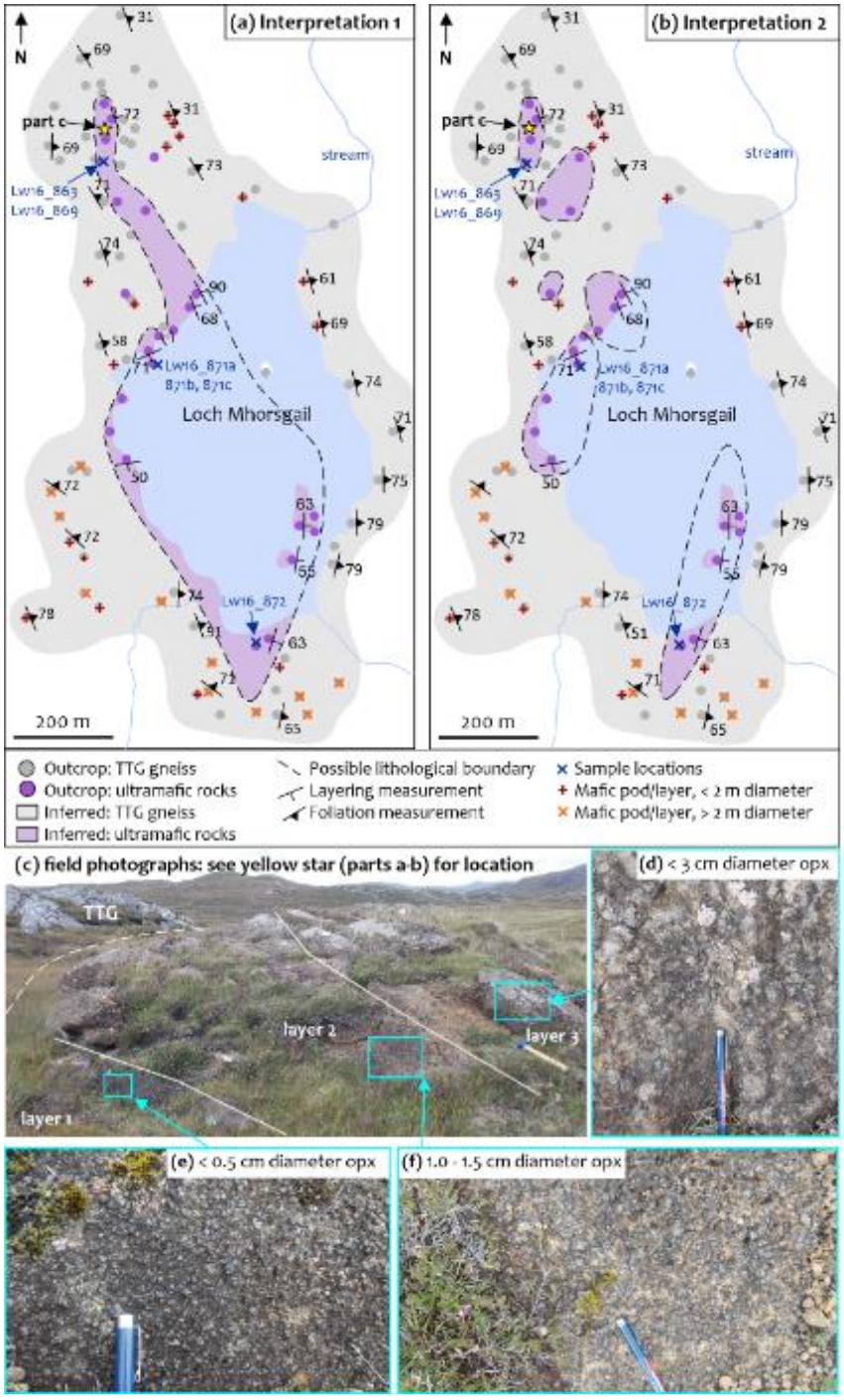

358

359 **Figure 4: (a-b)** Exposure maps of the Loch Mhorsgail Complex, with two potential interpretations for the lateral extent of the
360 ultramafic body. See Fig. 1b for its location in Lewis. **(c)** Field photograph detailing the outcrop-scale layering shown by the
361 Loch Mhorsgail Complex. **(d–f)** Smaller-scale field photographs detailing the grain size variation shown by different layers
362 shown in (c). Note: the different mapping style (relative to Figures 3, 5) used to account for the two possible interpretations.

3.3 Coltraiseal Mor

Ultramafic–mafic rocks at Coltraiseal Mor occur as three elliptical-shaped bodies that stand proud of the generally low-lying and poorly-exposed TTG gneisses (Fig. 5a). The largest ultramafic–mafic body is approximately 220 m x 160 m, while the smaller bodies are < 50 m diameter. The ultramafic–mafic rocks show dark-grey weathered surfaces that often show cm-scale pockmarks (Fig. 5b) and comprise pyroxene (predominantly orthopyroxene), olivine and plagioclase in variable proportions, alongside minor phlogopite (Fig. 5c). Subtle layering is present in rare outcrops, but no systematic variation in modal mineral proportions is identified across the mapped area. The TTG is of similar character to that described at nearby Loch Mhorsgail (Fig. 1b). The contacts between the ultramafic–mafic bodies and the surrounding TTG gneiss are not exposed, with the TTG foliation consistently parallel to the margins of the largest ultramafic–mafic body. Decimetre- to meter-scale pods/layers of mafic material rarely occur in the TTG gneiss, alongside common quartz-feldspar-biotite pegmatites.

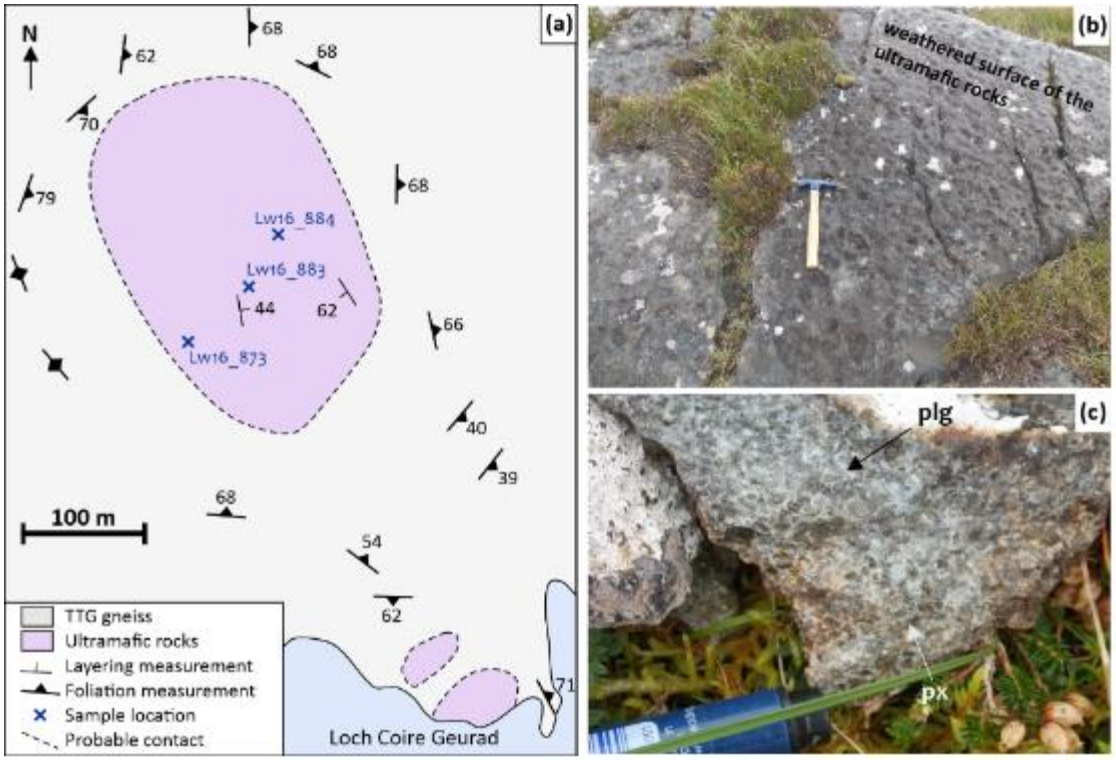

Figure 5: (a) Geological map of the Coltraiseal Mor ultramafic body. See Fig. 1b for its location in Lewis. **(b-c)** Field photographs detailing the weathered and fresh surfaces of the ultramafic rocks.

4.0 SAMPLES AND ANALYTICAL METHODOLOGY

A total of 15 samples were collected for this study, with 13 samples from the mapped ultramafic–mafic bodies at Maaruig (*n=4*), Loch Mhorsgail (*n=6*) and Coltraiseal Mor (*n=3*). An additional 2 samples were collected from the ultramafic–mafic body at Beinn a' Chuailean (see Fig. 1b for location in Lewis). Brief field observations of Beinn a' Chuailean qualitatively suggests it is similar to the exposures at Coltraiseal Mor (Section 3.3). Sample locations are provided in Table 1 and Figures 3–5. Further to thin sectioning, all samples were crushed and their major- and trace-element bulk-rock geochemistry analyzed. Thirteen of the samples also underwent PGE and Au bulk-rock geochemical analysis, with the methodologies employed described below.

4.1 Bulk-rock geochemistry: Major and trace elements

In preparation for bulk-rock geochemical analysis, weathered surfaces were removed using a diamond-bladed rock-saw, before samples were crushed using a Mn-steel jaw-crusher and ground using an agate ball mill at Cardiff University. Powdered samples were then ignited (at ~900°C) for 2 hours, with loss-on-ignition (LOI) determined gravimetrically.

A sample mass of 0.1 g was accurately weighed and mixed with 0.6 g of Li metaborate flux in a Claisse Pt-Rh crucible (see McDonald and Viljoen 2006). Approximately 0.5 mL of a Li iodide solution was added as a non-wetting agent, before the mixture was fused over a propane burner on an automated Claisse FLUXY fusion system. The mixture was dissolved in a Teflon beaker containing 50 ml of 4 % HNO_3, before the solution was spiked with 1 mL of a 100 ppm Rh spike solution (for use as an internal standard) and made up to 100 mL with 18.2 MΩ de-ionised water. Samples were then analyzed for major and trace elements using a Thermo iCAP 7000 series ICP-OES and Thermo X Series 2 ICP-MS (for solution analyses) respectively. Standard reference materials (SDO-1 and MRG1) and blanks were prepared and analyzed using the same method and instrumentation, with the sample material omitted for the blanks. Accuracy was constrained by analysis of international standard reference materials MRG1 and SDO-1, with precision (reported as the 2se – standard error) constrained by

403 conducting duplicate analyses of selected unknown samples (LW16_900 and LW16_905; see
404 supplementary material).

405 **4.2 Bulk-rock geochemistry: platinum-group elements and gold**

406 All samples were prepared by Ni sulphide fire assay followed by Te co-precipitation, with the full
407 method described by Huber et al. (2001) and McDonald and Viljoen (2006). Typically, 7.5 g of
408 powdered sample was mixed with 7.5 g of silica, 6 g of Na_2CO_3, 12 g of sodium tetraborate decahydrate
409 (borax), 0.9 g of sulfur and 1.1 g of carbonyl-purified Ni. After thoroughly mixing the reagents with the
410 unknown material, the samples were transferred to fire clay crucibles and fired at 1050°C for 90
411 minutes. The resulting sulphide buttons were dissolved using concentrated HCl, with co-precipitation
412 achieved using Te and $SnCl_2$. The filtered residues were digested using 4 ml of concentrated HCl and 3
413 ml of concentrated HNO_3 in 15 ml Saville screw-top Teflon vials. After the residue had dissolved, liquid
414 contents were transferred to 50 ml volumetric flasks spiked with a 2.5 ppm Tl spike, for use as an
415 internal standard. Samples were made up to 50 ml with 18.2 MΩ deionized water. Solutions were
416 analyzed for PGE and Au using a Thermo X Series 2 ICP-MS (for solution analyses) at Cardiff University.
417 Standard reference material (TDB1) and blanks were prepared and analyzed using the methodology
418 described above, with accuracy and precision (reported as the 2se – standard error) constrained by
419 the analysis of the international standard reference TDB1 (see supplementary material).

420 **5.0 RESULTS**

421 **5.1 Petrography**

422 *5.1.1 Maaruig*

423 The four Maaruig samples (Fig. 6a–b), which classify as metaperidotite and metapyroxenite (based on
424 modal mineral proportions; see Table 1), comprise olivine, orthopyroxene, clinopyroxene, amphibole
425 and spinel-group minerals, with accessory phlogopite. Olivine occurs as 0.3–3.5 mm diameter,
426 subhedral to anhedral grains that show limited alteration. Congruent with field observations (Section

3), orthopyroxene occurs as large, 3–14 mm diameter anhedral to subhedral grains. These grains commonly contain inclusions of anhedral, 0.2 mm diameter oxide phases and < 0.5 mm diameter silicate minerals (predominantly olivine, with rarer amphibole). Clinopyroxene is rare, occurring as 0.3–1.5 mm diameter subhedral grans that are amphibolitized, most notably along cleavage planes. Amphibole occurs as subhedral to euhedral, 0.1–0.8 mm in diameter grains that commonly show 120° triple junctions and appear to replace pyroxene. Spinel group minerals — classified as Al-chromite and picotite, with rare Fe-chromite and chromite — are 40–300 μm diameter and euhedral to subhedral.

5.1.2 Mhorsgail

The six Loch Mhorsgail rocks (Fig. 6c–d), which classify as metaperidotite and metapyroxenite and show slightly more visible alteration (to fine-grained amphibole) than the Maaruig rocks, comprise olivine, orthopyroxene, clinopyroxene, amphibole, and spinel group minerals in varied proportions (see Table 1), with accessory phlogopite, plagioclase, ilmenite, apatite and dolomite. Olivine forms 0.4–3.5 mm diameter grains that are subhedral to anhedral. Anhedral orthopyroxene grains are 3.5–15.0 mm in diameter and, like those at Maaruig, contain μm-scale spinel inclusions and mm-scale silicate inclusions (comprising olivine and amphibole). Clinopyroxene, which occurs rarely as cores rimmed by clusters of finer-grained amphibole, is subhedral and 1.0–1.5 mm in diameter. Amphibole is generally 0.1–1.0 mm in diameter and subhedral, with 120° triple junctions common, particularly between smaller grains. Plagioclase occurs rarely, forming anhedral grains 1.0–1.5 mm in diameter. Phlogopite occurs rarely as an accessory phase in some thin sections, forming elongate, pleochroic grains that are euhedral to subhedral and up to 1.5 mm in diameter. Spinel group minerals — classified as Al-chromite and picotite, with rare Fe-chromite and chromite — are 40–300 μm diameter and euhedral to subhedral.

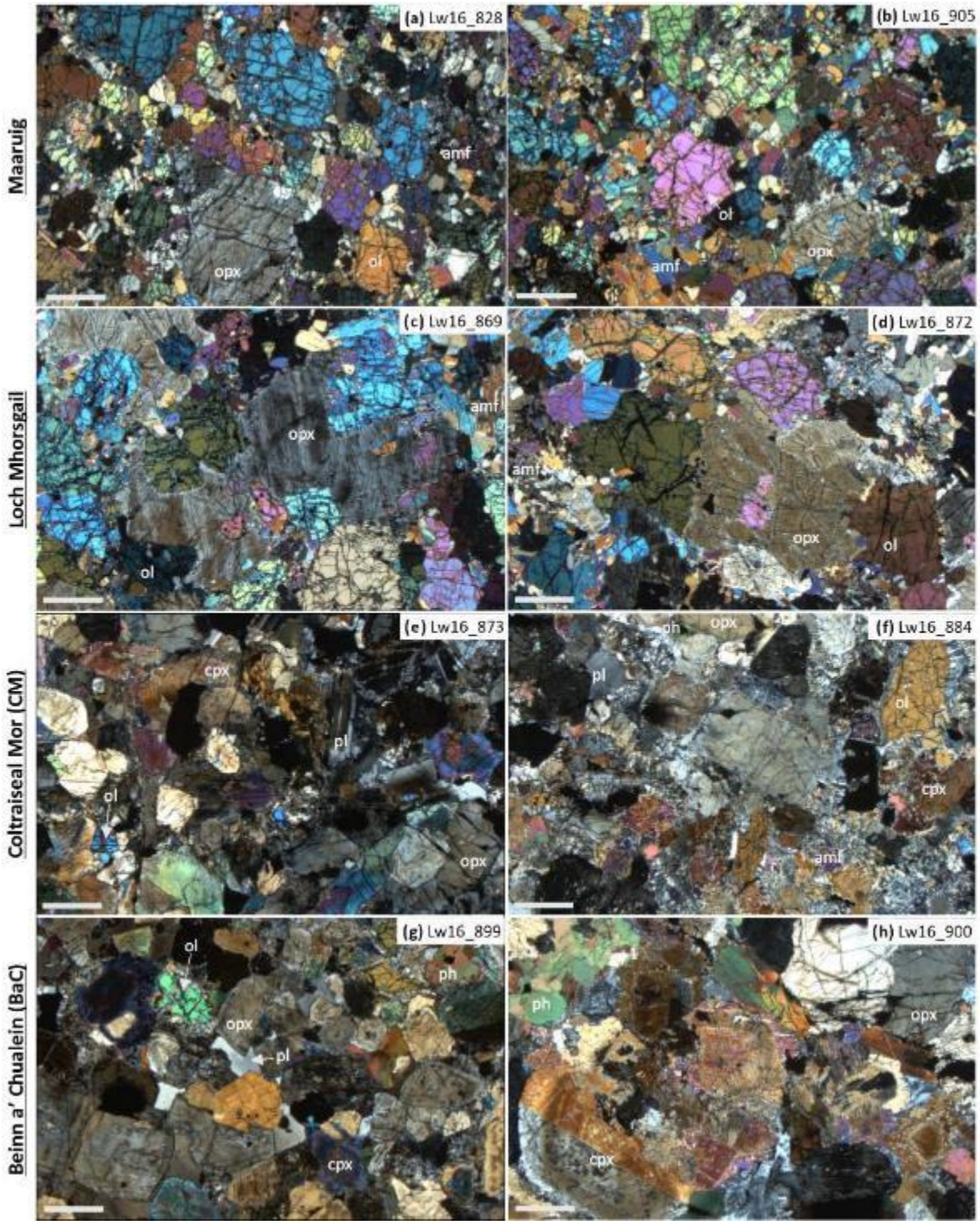

449

450 **Figure 6:** Crossed-polarised light (XPL) photomicrographs for the Maaruig (a-b), Loch Mhorsgail (c-d), Coltraiseal Mor (e-f)
451 and Beinn a' Chuailean (g-h) complexes. Abbreviations: amf = amphibole; cpx = clinopyroxene; ol = olivine; opx =
452 orthopyroxene; ph = phlogopite; pl = plagioclase. White scale bar = 1 mm. See main text for full petrographic descriptions
453 (Section 5.1).

454 *5.1.3 Coltraiseal Mor*

455 The three Coltraiseal Mor rocks (Fig. 6e–f), which classify as metagabbronorite, comprise olivine,
456 orthopyroxene, clinopyroxene, amphibole, plagioclase and phlogopite in varied proportions, with
457 accessory pyrrhotite, apatite, pyrite and Cr-spinel. Olivine is subhedral to anhedral and 0.3–2.5 mm in
458 diameter. Orthopyroxene is subhedral to anhedral, 1.0–3.2 mm in diameter and occasionally displays
459 weak pleochroism. Where present, clinopyroxene is subhedral to anhedral and < 3.2 mm in diameter,
460 with common alteration to fine-grained (µm-scale) amphibole. Amphibole also occurs as 0.5–2.5 mm
461 diameter, subhedral grains that show common 120° triple junctions. Highly pleochroic phlogopite is
462 0.1–2.0 mm diameter and anhedral, with subhedral plagioclase generally 0.8–2.5 mm in diameter.

463 *5.1.4 Beinn a' Chuailean*

464 The two Beinn a' Chuailean rocks (Fig. 6g–h), which classify as meta-olivine gabbronorite and
465 metagabbronorite, comprise olivine, orthopyroxene, clinopyroxene, amphibole, plagioclase and
466 phlogopite, with accessory ilmenite, apatite, Cr-spinel and pyrite. Olivine, which is 0.3–2.5 mm in
467 diameter and anhedral to subhedral, appears to cluster in specific parts of thin sections.
468 Orthopyroxene is 0.8–6.5 mm in diameter and subhedral, with some fine-grained alteration to
469 amphibole restricted to cleavage planes. Clinopyroxene occasionally preserves relic twinning and
470 zoning, with grains typically 0.8–3.0 mm in diameter and subhedral. Plagioclase is anhedral to
471 subhedral and 0.5–2.5 mm in diameter, while phlogopite is 0.2–3.5 mm in diameter and anhedral.

472 **5.2 Bulk-rock geochemistry**

473 Table 2 presents the major and trace element geochemistry of all samples analyzed in this study,
474 alongside key normalized trace element ratios. To assess potential correlations, our data are
475 compared to comparatively well-defined phases of ultramafic–mafic magmatism recorded in the
476 mainland LGC's Central Region (see Section 2.1). Specifically, we compare these data to: (i) a suite of
477 Paleoproterozoic mafic dykes, known as the "Scourie Dykes" (Hughes et al., 2014); (ii) a large group of
478 distinctly layered Archean ultramafic–mafic rocks (Guice et al. 2018b, 2020); and (iii) a smaller, more

enigmatic group of generally massive, peridotitic Archean ultramafic–mafic rocks (Guice et al. 2020). For descriptions of these phases of ultramafic–mafic magmatism, see Section 2.1. All LGC comparison data were collected using the same sample preparation procedures at Cardiff University (see Section 4) as for the present study. Also included for comparison — as an end-member — are global residual mantle rocks sampled from ophiolites and as oceanic peridotites (Godard et al., 2000, 2008; Paulick et al., 2006).

5.2.1 Major elements

The analyzed Outer Hebrides samples form two groups based on their MgO and SiO_2 contents, with this distinction correlating with sample location. The Maaruig and Loch Mhorsgail samples are more MgO-rich, containing 32–40 wt. % MgO and 40–47 wt. % SiO_2, while the Beinn a' Chuailean and Coltraiseal Mor samples are less MgO-rich, containing 19–24 wt. % MgO and 51–53 wt. % SiO_2. This geochemical distinction between the four localities can also be seen for most other major and minor elements (Fig. 7). Collectively, the Outer Hebridean samples form broadly linear trends on bivariate plots (Fig. 7), with MgO showing a strong negative correlation (R^2 = ≥ 0.7) with SiO_2, TiO_2, Al_2O_3, CaO and Na_2O, a moderate negative correlation (R^2 = 0.4–0.7) with K_2O, a strong positive correlation with Ni and Cr, and a weak positive correlation (R^2 = 0.1–0.4) with Fe_2O_3. A notable feature is the strong Cr enrichment shown by the Maaruig and Loch Mhorsgail samples relative to other analyzed samples and comparison data, which correlates with the higher modal percentages of spinel-group minerals (see Section 5.1; Table 1).

5.2.2 Trace elements

Figure 8 details the trace element compositions of the studied samples according to their MgO contents. The relatively MgO-poor samples from Coltraiseal Mor and Beinn a' Chuailean are generally enriched in trace elements relative to the MgO-rich samples from Maaruig and Loch Mhorsgail, but there is overlap in the absolute concentrations of all trace elements (Fig. 8). When considered

collectively, the two groups form broadly linear trends for most trace elements ($R^2 > 0.6$), with the exception of Th and Nb, which exhibit R^2 values of 0.2 and 0.3 respectively (Fig. 8).

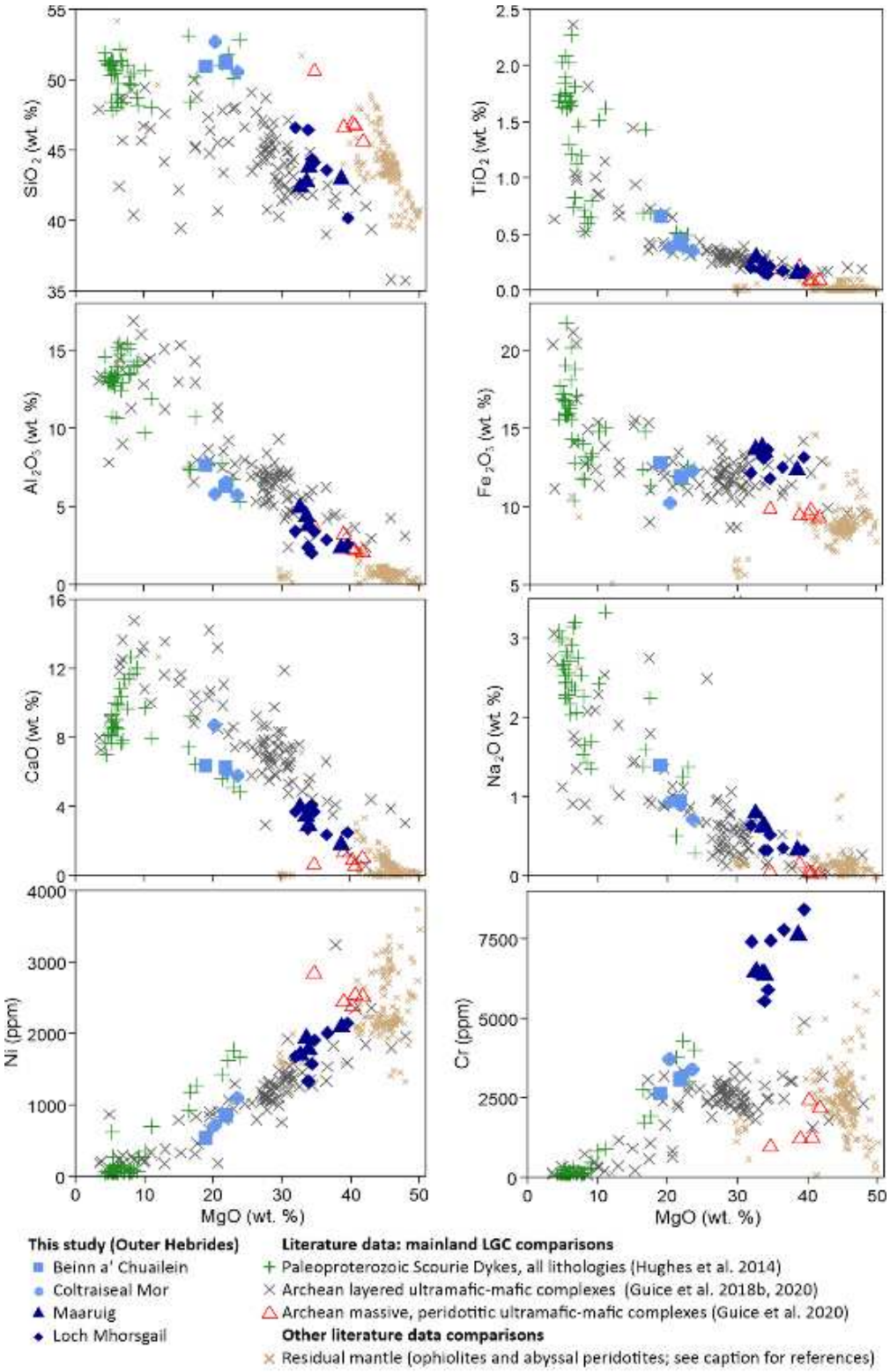

Figure 7: Bulk-rock major and minor element bivariate plots for the rocks analyzed as part of this study. These data are compared to the Paleoproterozoic Scourie Dykes and Archean ultramafic–mafic bodies exposed in the mainland LGC (see figure for references), and to residual mantle rocks (data from: Paulick et al. 2006, Godard et al. 2000, 2008).

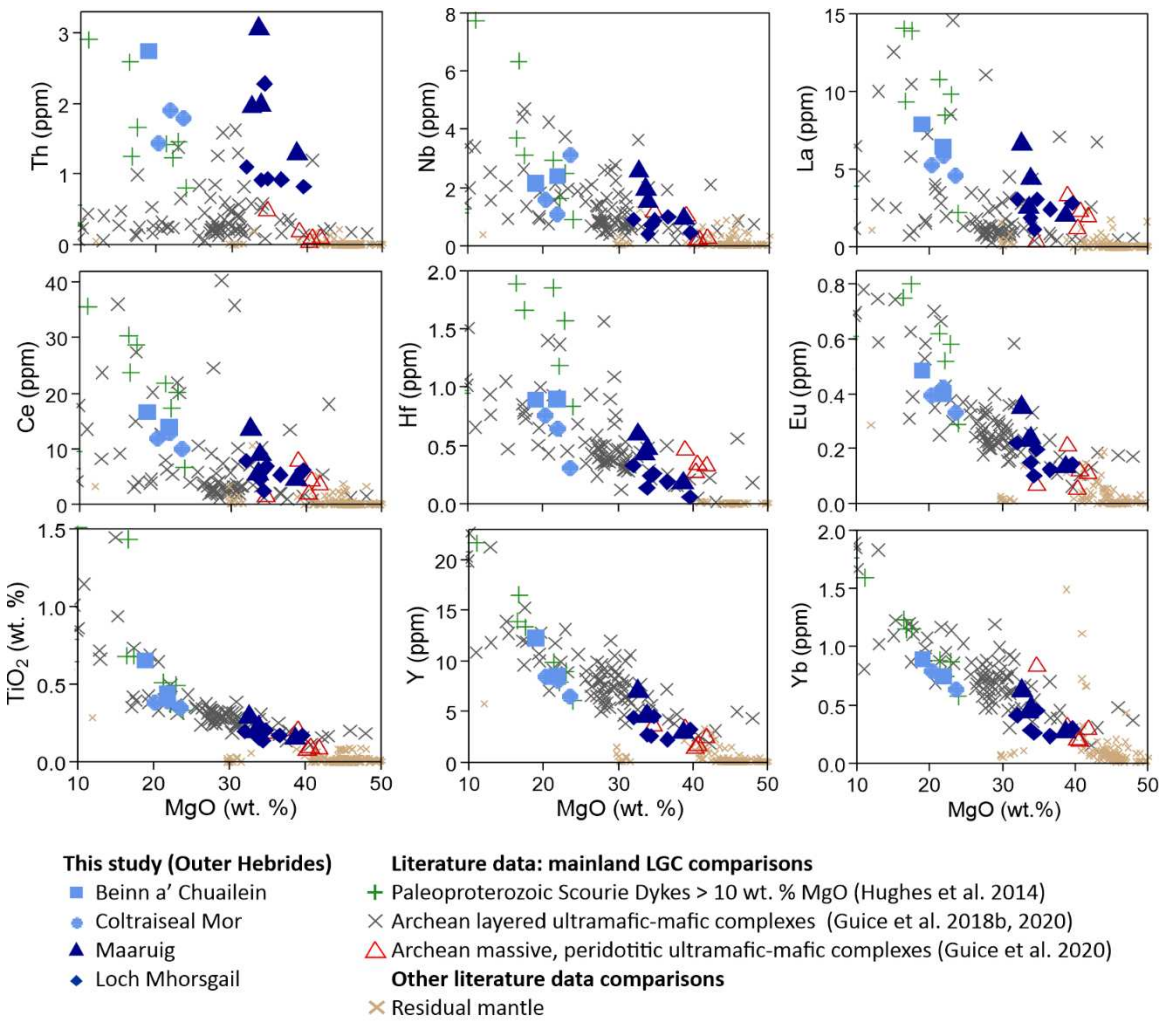

Figure 8: Bivariate plots detailing the trace element compositions of the studied ultramafic–mafic rocks, plotted against MgO. For data visualization purposes, the x axis is clipped to include the 10–50 wt. % MgO range.

On chondrite-normalized rare earth-element (REE) plots (Fig. 9a–d), all of the analyzed rocks from all four localities display relatively flat heavy-REE (HREE) patterns and negatively sloping light-REE (LREE) ($[La/Lu]_N$ = 2.4–8.3; $[La/Sm]_N$ = 1.7–3.9; Fig. 9a-d). The Maaruig and Loch Mhorsgail samples are comparatively depleted in all of the REE, displaying chondrite-normalized values of 1.2–27.9 (Fig. 9a–b), while the Coltraiseal Mor and Beinn a' Chuailean samples show chondrite-normalized values of 3.5–33.0 (Fig. 9c–d).

On primitive mantle-normalized trace element plots (Fig. 9e–h), the analyzed rocks from the Maaruig and Loch Mhorsgail Complexes show negatively sloping patterns ($[Th/Yb]_N$ = 11.5–48.8), prominent negative Nb-Ta anomalies ($[Nb/La]_N$ = 0.2–0.8), weak negative Zr-Hf-Ti anomalies and normalized

abundances ranging from 0.2 to 38.5 (Fig. 9e–f). The analyzed samples from the Beinn a' Chuailean and Coltraiseal Mor localities also show negatively sloping trace element patterns ([Th/Yb = 10.1–85.4), prominent negative Nb-Ta anomalies ($[Nb/La]_N$ = 0.2–0.7) and weak negative Zr-Hf-Ti anomalies, but are relatively enriched in all trace elements, with primitive mantle-normalized trace element abundances range from 0.8–144.6 (Fig. 9g–h). These data are also visualized on several bivariate plots (Fig. 10), which is a simpler visualization of the trace-element variation described in full by the normalized plots.

5.2.3 Platinum-group elements (PGE) and gold (Au)

On chondrite-normalized PGE (+Au) diagrams, the Maaruig Complex samples (*n=2*) display fractionated patterns ($[Pd/Ir]_N$ = 5.8–6.6), with flat Pd-group PGE (Pt, Pd, Rh; PPGE) and fractionated, positively sloping Ir-group PGE (Os, Ir, Ru; IPGE; Fig. 11a). The majority of Loch Mhorsgail samples (*n=6*) display flat to mildly fractionated chondrite-normalized PGE patterns ($[Pd/Ir]_N$ = 1.3–4.1), with one sample having an overall negative slope ($[Pd/Ir]_N$ = 0.2). They also define positive IPGE patterns and flat to negatively sloping PPGE (Fig. 11b). The Coltraiseal Mor samples (*n=3*) have flat to mildly fractionated chondrite-normalized PGE patterns ($[Pd/Ir]_N$ = 1.2–2.8), with flat to positively sloping IPGE and negatively to positively sloping PPGE (Fig. 11c). The Beinn a' Chuailean samples (*n=2*) define mildly fractionated patterns ($[Pd/Ir]_N$ = 1.8–2.8), with positively sloping IPGE and flat PPGE (Fig. 11d). These data are further visualized on the Ir versus chondrite-normalized Pd/Ir plot (Fig. 12). The Outer Hebridean samples show moderate scatter, with Ir contents ranging from 0.4 to 2.4 ppb, and Pd/Ir ratios ranging from 0.2 to 8.3.

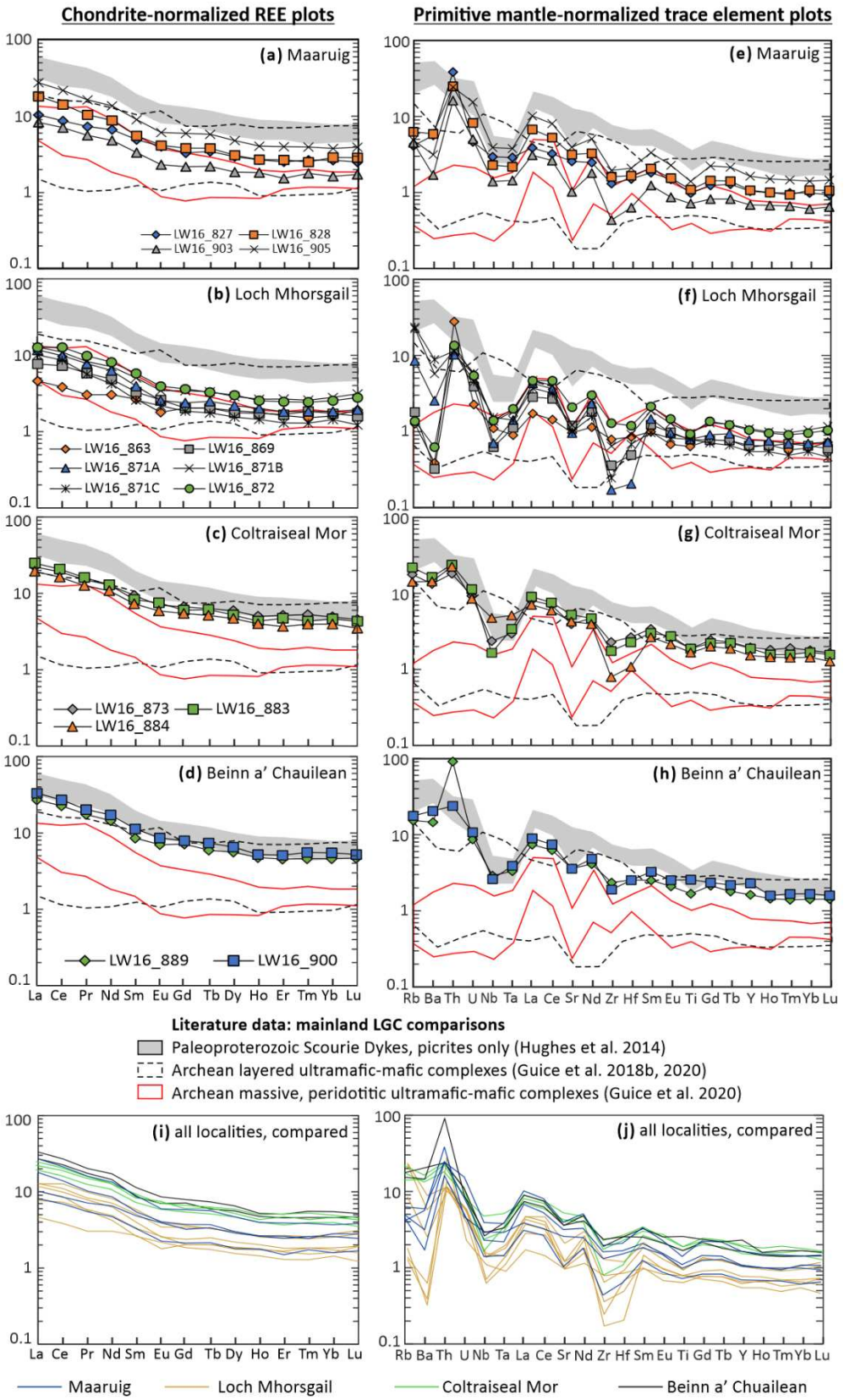

Figure 9: Chondrite-normalized (McDonough and Sun, 1995) REE plots (left-hand column) and primitive mantle-normalized (McDonough and Sun, 1995) trace element plots (right-hand column) for the Maaruig (a–b), Loch Mhorsgail (c–d), Coltraiseal Mor (e–f) and Beinn a' Chuailean (g–h) ultramafic–mafic bodies. (i–j) Comparison of all localities.

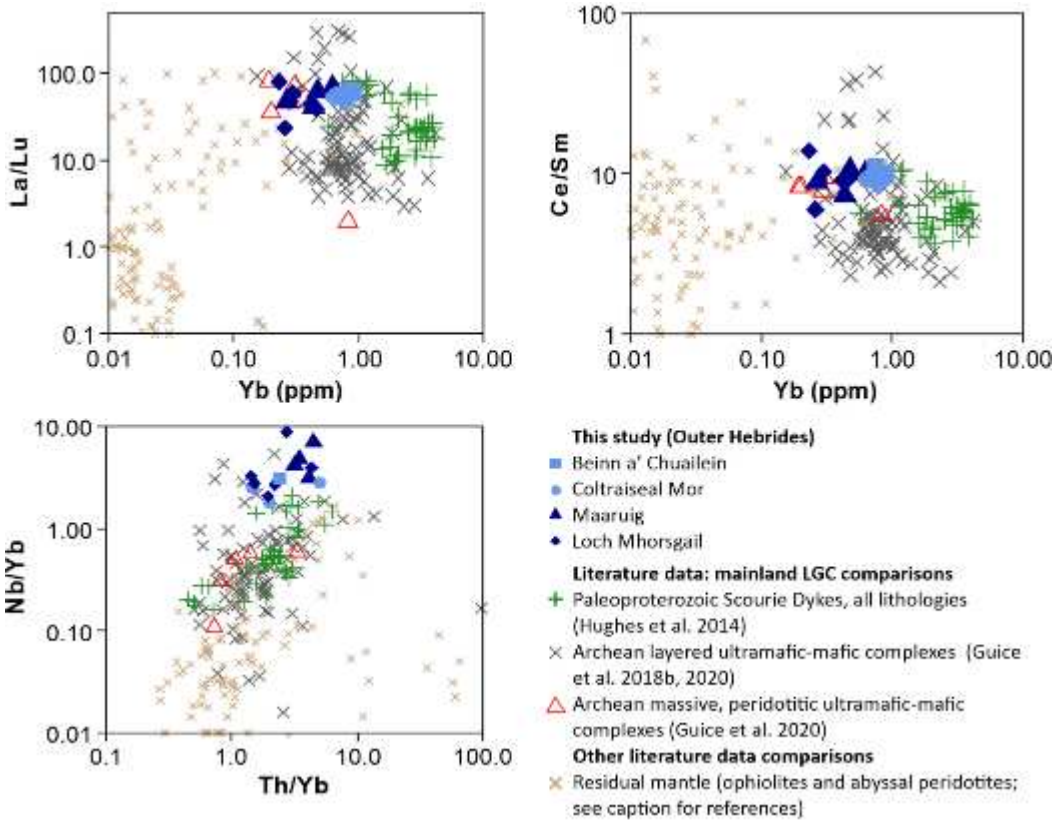

545

546 **Figure 10:** Yb versus La/Lu (a), Yb versus Ce/Sm (b) and Nb/Yb versus Th/Yb (c) bivariate plots for the rocks analyzed as part

547 of this study. Residual mantle rocks data: Paulick et al. (2006), Godard et al. (2000, 2008).

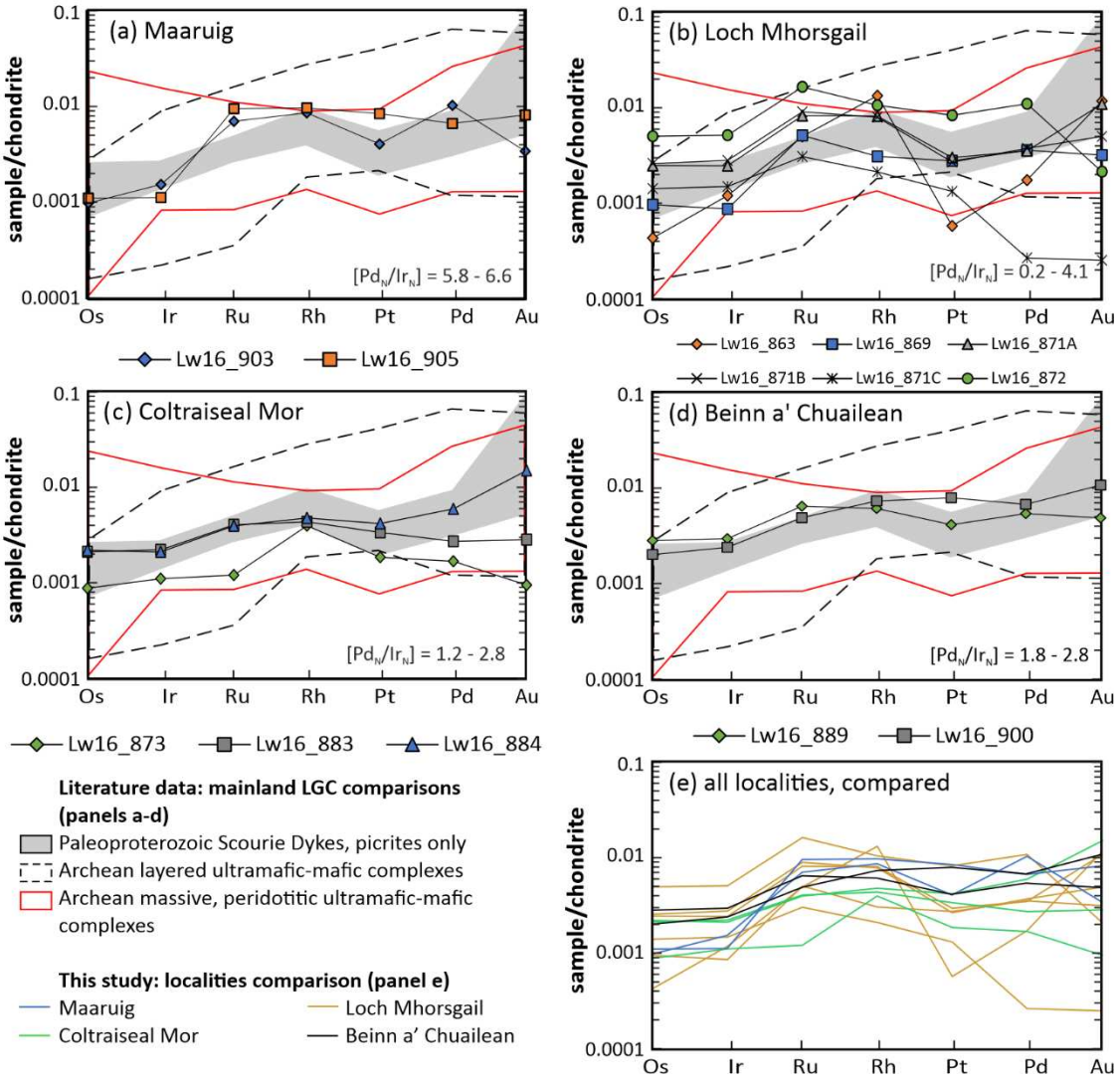

548

549 **Figure 11:** Chondrite-normalized (Lodders, 2003) platinum-group element (PGE) + Au plots for the analyzed ultramafic rocks.

550 References as in Fig. 9.

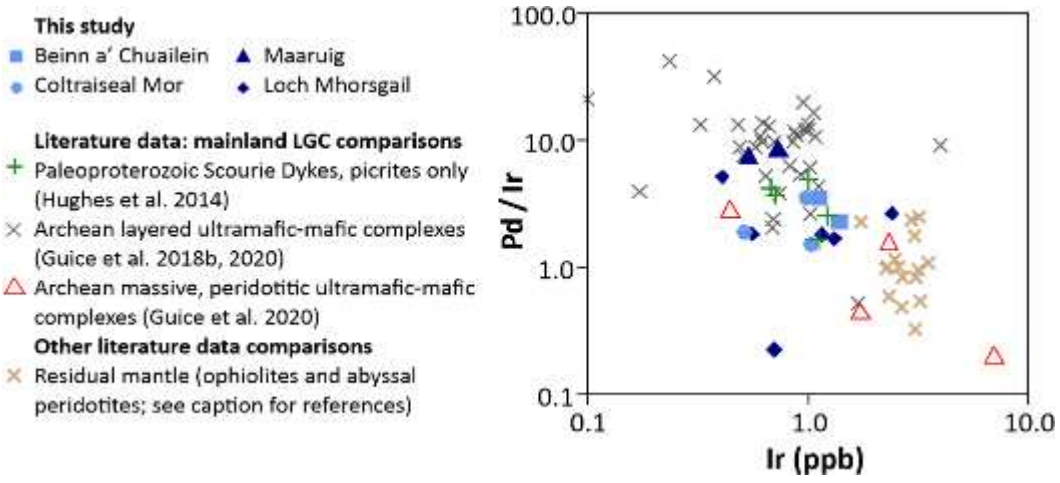

551

552 **Figure 12:** Ir versus Pd/Ir for the analyzed ultramafic rocks from the Outer Hebrides.

5.3 Comparisons with existing datasets

One end-member interpretation for ultramafic remnants in Archean cratons is that they represent fragments of ophiolitic mantle, with ophiolitic hypotheses proposed for a plethora of Archean–Paleoproterozoic ultramafic–mafic complexes globally (Kusky et al., 2001, 2007; Anhaeusser, 2006; Furnes et al., 2007; Polat et al., 2008; Grosch and Slama, 2017). The Maaruig, Loch Mhorsgail, Coltraiseal Mor and Beinn a' Chuailean complexes exhibit geochemical characteristics distinct from this field. The major and minor-element compositions show no overlap with the ophiolitic mantle and abyssal peridotites field on bivariate plots (Fig. 7); trace element compositions are enriched by several orders of magnitude relative to those of residual mantle rocks (Figs. 8–9); the bulk-rock Th/Yb and La/Lu ratios are high relative to residual mantle rocks (Fig. 10); and the PGE compositions exhibit relatively low Ir abundances and Pt/Ir ratios (Figs. 11–12).

Another possibility is that the studied Outer Hebridean ultramafic–mafic rocks represent direct equivalents of the large group of distinctly layered Archean ultramafic–mafic complexes exposed in the mainland LGC (see Section 2.1.1 for a full description; Fig. 2; Sills et al., 1982; Guice et al., 2018a, 2020). The analyzed samples show some overlap with the field for Archean layered complexes on major element bivariate plots, but exhibit relative enrichment in SiO_2 and Cr_2O_3, and relative depletion in Al_2O_3 and CaO (Fig. 7). There are also some similarities in the trace element bulk-rock geochemistry, with samples showing significant overlap with the range of normalized abundances with this field. However, the normalized patterns are distinctive from these Archean layered complexes on both the REE and trace element plots (Fig. 9). Whereas the layered complexes from the mainland LGC exhibit distinctly flat normalized REE and trace element patterns (Fig. 9; Guice et al. 2018b), the Outer Hebridean ultramafic rocks from all localities display negatively sloping LREE (Fig 9a–d) and consistent negative HFSE anomalies (Fig. 9e–h). This chemical distinction is further illustrated by the Yb versus Ce/Sm, Yb versus La/Lu and Nb/Yb versus Th/Yb plots (Fig. 10).

Alternatively, the assessed ultramafic–mafic rocks could be correlatives of the generally massive, peridotitic (Archean) complexes in the mainland LGC (see: Guice et al., 2020; Section 2.1.1). On major element bivariate plots, the analyzed rocks are distinct from the small suite of samples for generally massive, peridotitic complexes, displaying relative depletion in SiO_2, MgO and Ni, and relative enrichment in TiO_2, Fe_2O_3, CaO, Na_2O and Cr_2O_3. There are some similarities in the normalized REE and trace element patterns shown by the Maaruig and Loch Mhorsgail samples (Fig. 9), with negatively sloping LREE patterns, negative HFSE anomalies and partial overlap with the field for generally massive, peridotitic complexes. However, these samples also show some differences, including relative enrichments in the HREE, some HFSE (e.g., Nb and Ta) and most incompatible elements (e.g., Rb, Th). Moreover, the Coltraiseal Mor and Beinn a' Chuailean samples show little or no overlap with this field on normalized REE and trace element plots (Fig. 9c–d, g–h). Samples also show limited overlap with this group of Archean ultramafic-mafic complexes on most trace element bivariate plots (Fig. 8), and on the Nb/Yb versus Th/Yb plot (Fig. 10c).

Finally, the studied ultramafic–mafic rocks in Lewis and Harris could be direct equivalents of the Paleoproterozoic (ca. 2.4 Ga) Scourie Dykes exposed in the mainland LGC (see Section 2.1.2), as proposed by several previous authors (e.g., Myers and Lisle, 1971; Davies et al., 1975). The most MgO-poor samples analyzed as part of this study — from the Coltraiseal Mor and Beinn a' Chuailean complexes — share some geochemical characteristics with the most magnesian mainland Scourie Dykes (classified as picrites). This geochemical similarity can be seen in terms of: major element compositions, with the exception of Ni (Fig. 7); chondrite-normalized REE patterns and normalized REE abundances (Fig. 9c–d); primitive mantle-normalized trace element patterns, which includes negative HFSE anomalies (Fig. 9g–h); and mildly fractionated ($[Pd/Ir]_N$ = 1.2–2.8) PGE patterns (Fig. 11c–d; Fig. 12). However, while the patterns are parallel to the field for MgO-rich mainland Scourie Dykes, the Coltraiseal Mor and Beinn a' Chuailean complexes show a small depletion (relative to the MgO-rich mainland Scourie Dykes) in almost all elements on normalized REE and trace element plots (Fig. 9).

In contrast, the samples from Maaruig and Loch Mhorsgail are geochemically distinct from the mainland Scourie Dykes. They are considerably more magnesian (> 30 wt. % MgO) than the most MgO-rich Scourie Dykes (< 24 wt. % MgO) and show differences in the abundance of most other major elements (Fig. 7). Moreover, samples from these two localities exhibit significant depletion in all trace elements relative to the Scourie Dyke picrites, as illustrated on the trace element bivariate plots (Figs. 8, 10), chondrite-normalized REE plot (Fig. 9a–b) and primitive mantle-normalized trace element plots (Fig. 9e–f).

6.0 DISCUSSION

6.1 Mapping, field observations and relative age constraints

Myers and Lisle (1971) described the ultramafic–mafic bodies in Lewis and Harris as small (generally < 0.5 km^2) lenses and remnants that can be broadly divided into the following two groups based on lithological characteristics: (1) mafic rocks — comprising < 0.5 cm diameter clinopyroxene and hornblende "clots", alongside a plagioclase-dominated groundmass — that show relatively homogenous textures and no evidence for layering or chilled margins; and (2) coarse-grained, layered ultramafic–mafic rocks, comprising olivine, orthopyroxene, clinopyroxene, plagioclase and hornblende in variable proportions, alongside minor chromite and phlogopite. Other research conducted by Mason and Brewer (2004) describes a suite of mafic dykes concentrated in Harris that comprise hornblende, plagioclase and quartz, with these occurrences reportedly cross-cutting the TTG gneiss. Most of these ultramafic–mafic rocks in Lewis and Harris are considered younger than the TTG (e.g., Myers and Lisle, 1971), but selected occurrences have been suggested to pre-date the TTG gneiss based on their chaotic distribution within the TTG gneiss (e.g., Mason and Brewer 2004). Fettes and Mendum (1987) describe "Younger Basics" and "Older Basics", which are interpreted as correlatives of the mainland Scourie Dykes and layered bodies that pre-date the TTG protoliths respectively. In this section, we place the Maaruig, Loch Mhorsgail, Coltraiseal Mor and Beinn a' Chuailean bodies within

626 the context of these previous studies, and consider the relative age relations with the surrounding
627 lithologies.

628 *6.1.1 Maaruig and Loch Mhorsgail*

629 The metaperidotite and metapyroxenite samples from Maaruig and Loch Mhorsgail have a mineralogy
630 (Table 1; Section 5.1) comparable to the Group 2 occurrences described by Myers and Lisle (1971; see
631 above). This correlation is supported by other aspects of the field characteristics, such as the
632 prominent brown weathered surfaces that stand proud of the surrounding TTG gneiss, and presence
633 of layering on mm-, cm-, dcm-, and m-scales (Section 3; Figs. 3 and 4). These group 2 ultramafic–mafic
634 bodies have previously been considered to represent deformed Paleoproterozoic dykes that are
635 possibly correlatives of the mainland Scourie Dykes (Fig. 2; Myers and Lisle 1971), with this broad
636 hypothesis potentially supported by a ca. 2.1 Ga Sm-Nd (bulk-rock) isochron age yielded from a mafic
637 rock collected from the Maaruig area (Cliff et al. 1998). However, the sample location reported does
638 not correlate with the area mapped here. Rather, our field mapping and observations suggest that the
639 Maaruig and Loch Mhorsgail bodies could be older than or broadly coeval with the local TTG gneiss.
640 This interpretation is supported by the map-scale discordance between the ultramafic layering and
641 lithological contacts at both localities (Figs. 3 and 4); and by the presence of meter-scale mafic pods
642 in the TTG immediately adjacent to the ultramafic–mafic bodies at Loch Mhorsgail (Fig. 4), which could
643 reflect intrusion by the TTG protoliths or sagduction of ultramafic–mafic material into partially molten
644 TTG (see Johnson et al. 2016 and references therein).

645 Although these observations are not irrefutable evidence of a pre-TTG origin for Maaruig and Loch
646 Mhorsgail, an important comparison with the Archean layered bodies of the LGC's mainland can be
647 made, with these occurrences likely post-dating the local TTG gneiss protoliths (Burton et al., 2000;
648 Guice et al., 2018a). This group of mainland ultramafic–mafic complexes exhibit consistent
649 concordance between layering, lithological contacts and the TTG foliation, despite being considerably
650 more deformed that the Maaruig and Loch Mhorsgail bodies studied here (Guice et al., 2020).

Similarly, there is no spatial relationship between the mainland ultramafic–mafic bodies and meter-scale mafic pods in the surrounding TTG, which is a notable feature of the Loch Mhorsgail occurrence. A pre-TTG hypothesis is therefore considered to be more likely than an interpretation whereby these occurrences represent deformed Paleoproterozoic dykes.

6.1.2 Coltraiseal Mor and Beinn a' Chuailean

The metagabbronorite and meta-olivine gabbronorite samples from Coltraiseal Mor and Beinn a' Chuailean also contain olivine, orthopyroxene, clinopyroxene amphibole and plagioclase, alongside minor oxide minerals and phlogopite, suggesting that they may also correlate with the Group 2 occurrences of Myers and Lisle (1971). However, there are some differences in the field characteristics shown by the Coltraiseal Mor and Beinn a' Chuailean bodies. This includes: relatively homogenous modal mineral proportions between samples (Table 1); presence of plagioclase and phlogopite as major mineral phases (Fig. 6; Table 1); absence of distinctive mineralogical layering on any scale; and consistent parallelism between TTG foliation and lithological boundaries. This raises the possibility that the Coltraiseal Mor and Beinn a' Chuailean bodies represent a different age relationship with the TTG gneiss (and thus record a distinct petrogenesis) to that favoured for Maaruig and Loch Mhorsgail (Section 6.1.1).

6.2 Metamorphism and element mobility

Irrespective of the age relations with the TTG gneiss, the studied ultramafic–mafic bodies have all been subject to at least one period of metamorphism: the 1.9–1.6 Ga greenschist–amphibolite-facies Laxfordian tectonothermal event (Fig. 2). This event resulted in local migmatization of the TTG gneiss and the intrusion of associated granites and pegmatites (Dearnley, 1962; Davies et al., 1975; Fettes and Mendum, 1987; Shaw et al., 2016), with such effects most pervasive in the northern and western parts of Lewis (Fig. 1).

In the studied thin sections, metamorphic re-crystallization is evidenced by 120˚ triple junctions shown by 0.5–2.0 mm diameter amphibole grains from all localities (Fig. 6). These rocks show limited

676 petrographic evidence for alteration, with olivine extremely fresh (Fig. 6a–d) and clinopyroxene zoning
677 sometimes preserved (Fig. 6e, g–h). Some samples show slightly more petrographic evidence of
678 alteration (e.g., Lw16_884 from Coltraiseal Mor), which manifests as amphibolitization of
679 clinopyroxene and sericitization of plagioclase (Fig. 6f). However, fresh olivine, pyroxene and
680 plagioclase are all preserved even in the most visibly altered samples.

681 This petrographic evidence, which suggests that the samples studied here have been subject to
682 relatively limited hydrothermal alteration, is supported by the bulk-rock trace element data. Within
683 suites of co-genetic samples, the relative mobility of trace elements can be tested by plotting
684 individual elements against those considered to be most immobile (e.g., Zr, Y and Yb) and calculating
685 the R^2 value (Fig. 13; e.g., Cann, 1970; Guice, 2019). Given the possibility that the Maaruig and Loch
686 Mhorsgail bodies were derived from a phase of magmatism distinct from Coltraiseal Mor and Beinn a'
687 Chuailean (see Section 6.1), R^2 values are given (and element mobility tested) for these groups
688 separately (Fig. 13). We here use the samples from Maaruig and Loch Mhorsgail to assess element
689 mobility, as they comprise 10 of the 15 samples assessed as part of this study and are therefore more
690 statistically robust.

691 When plotted against Zr on bivariate plots (Fig. 13), a selection of elements, including Yb, Y, Eu and
692 Hf, show high R^2 values ($R^2 \geq 0.7$) for the Maaruig and Loch Mhorsgail samples. This suggests that these
693 elements have experienced limited bulk-rock element mobility due to metamorphism and
694 hydrothermal alteration. A second group of elements — including TiO_2, La, Ce, Nb, Ta and Th — show
695 moderate correlations ($R^2 = 0.4–0.7$) with Zr that likely reflect small amounts of element mobility. The
696 interpretation of these elements as having experienced limited element mobility during
697 metamorphism is supported by the lack of correlation between trace element composition and
698 amphibole modal abundance, which is a phase derived from the alteration of clinopyroxene (see
699 Section 5.1). Samples LW16_873 and LW16_889 contain 45 modal % and 15 modal % amphibole

respectively, but exhibit near-identical normalized trace-element patterns for the elements considered immobile or as having experienced limited mobility (Fig. 9).

A final group of elements — Rb (R^2 = 0.11), Ba (R^2=0.0) and Cu (R^2 = 0.01) — display poor correlations with Zr (Fig. 13). Given their poor correlation with Zr, these elements likely experienced significant element mobility, with abundances in the studied rocks not reflective of primary magmatic compositions. As such, genetic interpretations are not based on these elements. Taken together, the studied ultramafic–mafic samples have experienced relatively limited bulk-rock element mobility as a consequence of metamorphism and associated hydrothermal alteration.

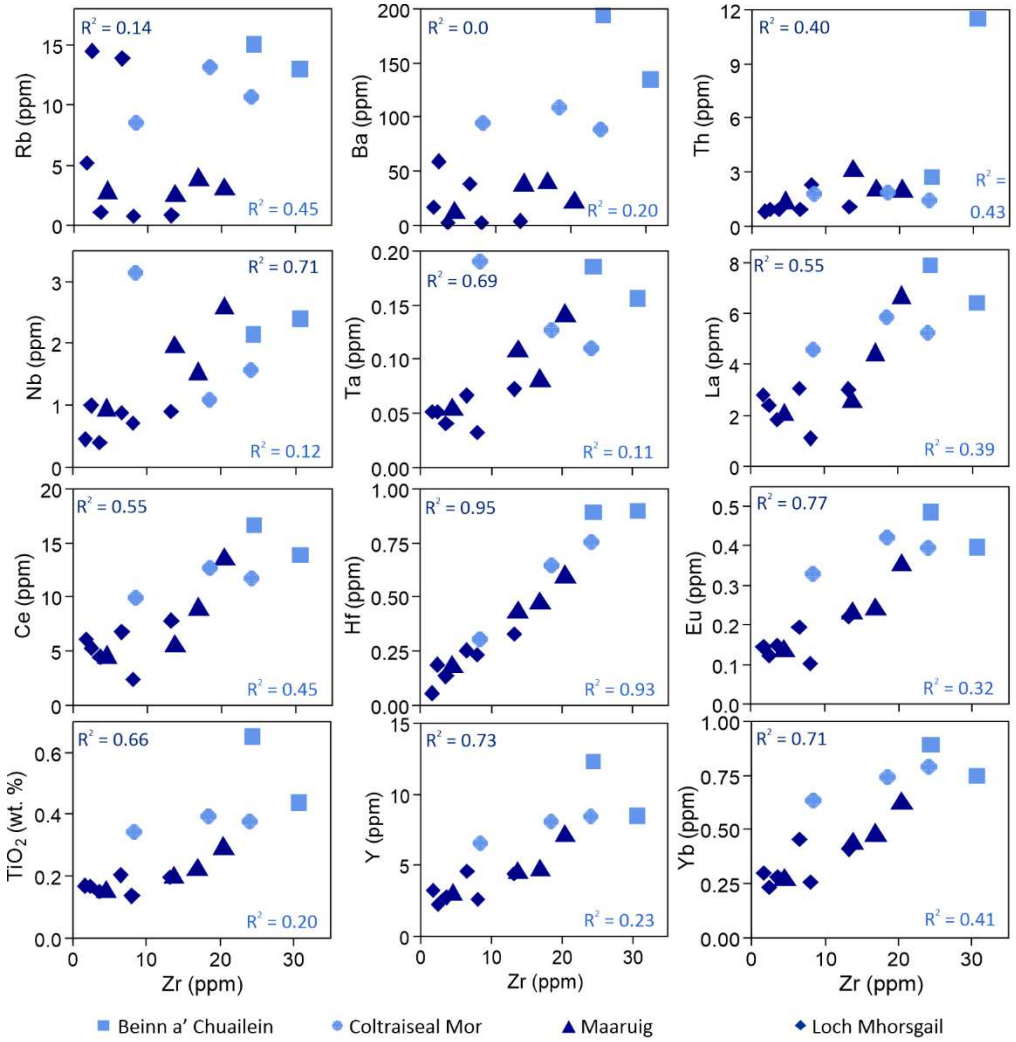

Fig. 13: Bivariate plots detailing the correlation between Zr and various trace elements. Separate R^2 values are provided for Maaruig and Loch Mhorsgail (dark blue), and for Coltraiseal Mor and Beinn a' Chuailean (light blue).

6.3 Petrogenesis of the studied ultramafic–mafic bodies

Ultramafic rocks can be produced in a variety of geological and tectonic environments, with several of these hypotheses proposed for ultramafic–mafic rocks exposed in the mainland LGC. This includes, but is not limited to: the lower portions of ophiolites/ oceanic lithosphere, including the mantle portion (Park and Tarney, 1987; Guice et al., 2020); komatiites that once formed part of a greenstone belt and were sagducted into the TTG (Johnson et al., 2016); cumulates, whose parental magmas could potentially be derived from several tectonic environments (Bowes et al., 1964; Guice et al., 2018a); or extension-related dykes (Hughes et al., 2014 and references therein).

In this section, we discuss the origin of the Maaruig, Loch Mhorsgail, Coltraiseal Mor and Beinn a' Chuailean bodies, and consider potential correlations with ultramafic–mafic rocks exposed in the mainland LGC's Central Region (see Section 2.1 for descriptions of these rocks). A comparison between the data presented here and various global/regional-scale datasets is provided in Section 5.3. Based on the chemical distinction between all analyzed ultramafic–mafic rocks studied here and residual mantle rocks, we consider it improbable that any of the analyzed samples are fragments of ophiolitic mantle. This hypothesis is therefore not considered in the succeeding sections.

6.3.1 Maaruig and Loch Mhorsgail

As discussed in Section 6.1, we consider it most likely that the Maaruig and Loch Mhorsgail bodies are older than or coeval with the local TTG gneiss. This Archean-age interpretation contradicts the broad hypothesis that these rocks represent deformed Paleoproterozoic dykes and, by extension, questions any direct correlation with the mainland Scourie Dykes (Dearnley, 1962; Myers and Lisle, 1971; Davies et al., 1975; Fettes and Mendum, 1987; Cliff and Rex, 1989). Moreover, other field and geochemical evidence contradict a direct equivalence between the Scourie Dykes and the Maaruig/Loch Mhorsgail bodies. While subtle layering is present in some Scourie Dykes, the scale and prominence of the layering presented in the Maaruig and Loch Mhorsgail bodies (Section 3.1–3.2) is not observed in the Scourie Dykes. The Maaruig and Loch Mhorsgail samples are also extremely MgO-rich (> 30 wt. %

MgO). For comparison, most previously analyzed Scourie Dykes generally contain < 10 wt. % MgO, with a small group of picrites containing 15–25 wt. % MgO (Fig. 7).

Instead, both Maaruig and Loch Mhorsgail exhibit several features characteristics of cumulates, with evidence for *in-situ* fractionation demonstrated by the distinctive modal layering observed on mm-, cm-, dcm- and m-scales. *In-situ* fractionation is also evidenced by the chemical data, with most major elements correlated with MgO (see Fig. 7), alongside fractionated PGE patterns (Fig. 11a–b). Given this interpretation, it is unlikely that these ultramafic bodies can be correlated with the "generally massive, peridotitic" (Archean) complexes exposed in the mainland LGC (see Section 2.1), with this distinction supported by the chemical data (see Section 5.3). It is, however, potentially suggestive of a correlation with the Archean "layered" complexes from the mainland LGC (see Fig. 2). Like this group of Archean ultramafic–mafic rocks, the Maaruig and Loch Mhorsgail occurrences display distinctive mineralogical layering on a variety of scales (Sills et al., 1982; Guice et al., 2018a). There are also some chemical similarities, with significant overlap with the field for Archean layered complexes on normalized REE and trace element plots (Fig. 9).

Despite this overlap, the flat patterns shown by the "layered" mainland ultramafic–mafic complexes are distinct from the patterns shown by the Maaruig and Loch Mhorsgail samples, which exhibit distinctive negative HFSE anomalies and LREE enrichment. Moreover, other aspects of the field relationships are distinct from this group. Rather than forming relatively thin (on a scale of tens of metres) units that can be traced for several hundred meters along strike (Guice et al., 2018a), the Maaruig and Loch Mhorsgail rocks occur as elliptical-shaped pods that exhibit discordance between layering and lithological contacts (see Section 6.1). As such, we consider it unlikely that the studied Outer Hebridean ultramafic–mafic bodies are direct equivalents of the layered complexes exposed in the mainland LGC, and Maaruig and Loch Mhorsgail may thus represent a distinct type of ultramafic–mafic magmatism in the LGC that is currently recognized only in the Outer Hebridean islands west of the OHFZ.

761 An alternative hypothesis is that the Maaruig and Loch Mhorsgail bodies represent cumulates that are
762 genetically related to the Scourie Dykes. However, as well as being unlikely based on the favoured age
763 relationships (Section 6.1), this interpretation is inconsistent with normalized trace element patterns
764 shown by the Maaruig and Loch Mhorsgail samples. These samples exhibit negative HFSE anomalies
765 and are parallel with those of the Scourie Dykes, but are depleted in all trace elements relative to this
766 field (see Fig. 9). If they were cumulate parents of the melts that formed the Scourie Dykes,
767 complimentary geochemical signatures would be expected, rather than the parallel patterns observed
768 (Charlier et al., 2005; Ma et al., 2016; Schaen et al., 2017). For example, ultramafic cumulates from
769 the Nincheng complex (North China Craton) are highly depleted in Sr and LREE, with the derivative
770 melts (preserved as adakites) exhibiting relatively high Sr/Y and La/Yb ratios (Ma et al., 2016).

771 The distinctive negative HFSE anomalies — alongside the associated LREE enrichment shown by all of
772 the analyzed samples from Maaruig and Loch Mhorsgail (as well as Coltraiseal Mor and Beinn a'
773 Chuailean) — are a bulk-rock geochemical signature that could reflect one or more of the following
774 potential origins: (a) parental magmas derived from subduction-related processes (Klemme et al.,
775 2005); (b) crustal contamination during magma ascent (Arndt, 1999); (c) secondary processes, such as
776 interaction with hydrothermal fluids (Lahaye et al., 1995); (d) cumulate effects, whereby LREE-rich
777 minerals are concentrated in these specific layers/units whilst the HFSE have been retained in the
778 residual magma; and (e) parental magmas partially derived from a previously metasomatized sub-
779 continental lithospheric mantle (Hughes et al., 2014). While it is not possible to assess these
780 hypotheses robustly using the data presented here, several comments can be made. First, as the
781 Maaruig and Loch Mhorsgail rocks are considered to have experienced limited element mobility (see
782 Section 6.2), hypothesis (c) is considered unlikely, but is not completely ruled out given the small
783 sample set and potentially cryptic effects of hydrothermal alteration in Archean cratons (Guice et al.,
784 2018b). Second, no distinctly LREE-rich mineral phases are identified in the Maaruig and Loch
785 Mhorsgail samples. Given the evidence for limited hydrothermal alteration, which is a process capable
786 of generating LREE enrichment (Rollinson and Gravestock, 2012; Guice et al., 2018b), hypothesis (d) is

787 also considered improbable, but not ruled out. It is therefore likely that the distinctive geochemical
788 signature is derived from the parental magma, but the specific process(es) responsible remains an
789 open question.

790 *6.3.2 Coltraiseal Mor and Beinn a' Chuailean*

791 One hypothesis is that these two ultramafic–mafic bodies are genetically related to the ultramafic
792 rocks at Maaruig and Loch Mhorsgail, with all occurrences representing variably fractionated products
793 of the same parental magma. Despite the aforementioned differences in field characteristics (see
794 above; Section 6.1), this hypothesis is potentially supported by some of the petrographic and chemical
795 characteristics. The mineral assemblage is broadly comparable to Maaruig and Loch Mhorsgail, with
796 the main differences being the prevalence of clinopyroxene, plagioclase and phlogopite in the
797 Coltraiseal Mor and Beinn a' Chuailean samples, which could potentially be attributed to magmatic
798 differentiation. Moreover, the chondrite-normalized REE and primitive mantle-normalized patterns
799 shown by all four localities studied here are parallel to one another.

800 Alternatively, there are several geochemical similarities between the Coltraiseal Mor and Beinn a'
801 Chuailean samples and the mainland Scourie Dykes (Section 5.3), raising the alternate possibility that
802 these occurrences are Outer Hebridean equivalents of this well-documented suite of ca. 2.4 Ga dykes
803 exposed in the mainland LGC (Fig. 2; Section 2.1.2). This hypothesis is potentially supported by the
804 favoured age relationship with the TTG gneiss (see Section 6.1), and by several field characteristics.
805 Unlike Maaruig and Loch Mhorsgail, Coltraiseal Mor and Beinn a' Chuailean show relatively consistent
806 modal mineral proportions between samples, alongside an absence of modal mineralogical layering.
807 On balance, we consider this latter hypothesis more likely, whereby the Coltraiseal Mor and Beinn a'
808 Chuailean are Paleoproterozoic dyke fragments that could be direct equivalents of the Scourie Dykes
809 exposed on the mainland.

6.4 Implications for the Lewisian Gneiss Complex, North Atlantic Craton

This study identifies a new phase of Archean ultramafic–mafic magmatism in the LGC: a suite of Archean cumulates in the Outer Hebrides of Lewis and Harris, as represented by the Maaruig and Loch Mhorsgail bodies. In terms of their field, petrographic and geochemical characteristics, these occurrences are distinct from any of the Archean ultramafic–mafic magmatism currently described in the mainland LGC's well-studied Central Region (see Section 2.1). This raises the possibility that Lewis and Harris (west of the OHFZ) formed a distinct crustal block that was separate from the mainland LGC's Central Region during the Mesoarchean, although the implications of this finding are open to interpretation. These two (or more) crustal blocks could have been separate terranes during the Mesoarchean, with their unique magmatic evolutions during this Era reflective of their origin as separate (micro)continents (e.g., Mason and Brewer, 2004; Kinny et al., 2005; Love et al., 2010). Alternatively, it is possible that the distinctive Mesoarchean evolution reflects heterogeneity within a once continuous piece of Archean crust.

In either case, the interpretation of the Coltraiseal Mor and Beinn a' Chuailean bodies as deformed Paleoproterozoic dykes that could be correlatives of the mainland LGC Scourie Dykes — as is considered most likely (see Section 6.3.2) — suggests that the Outer Hebrides (west of the OHFZ) and mainland portions of the LGC were proximal to one another by ca. 2.4 Ga. This hypothesis is consistent with recent U-Pb zircon geochronology conducted by Davies and Heaman (2014), who assigned a 2.41 Ga crystallization age to the Cleitichean Beag Dyke, which is located in central Lewis and is considered to be an Outer Hebridean "Scourie Dyke" (Fig. 1b). When combined with the identification of a distinct phase of Archean ultramafic–mafic magmatism in Lewis and Harris (represented by Maaruig and Loch Mhorsgail), this finding suggests that a major tectonic juxtaposition — whether via. subduction-accretion or large-scale crustal faulting — likely occurred in the LGC in the Neoarchean or early Paleoproterozoic prior to 2.42 Ga.

6.5 Ultramafic–mafic rocks: a crucial component of the early Earth puzzle

As described in the introduction to this paper, the Archean–Paleoproterozoic evolution of the LGC is described by competing models, including end-member models whereby it is interpreted to represent: (a) a section of broadly continuous Archean crust (Park and Tarney, 1987); or (b) multiple geologically unique terranes assembled via plate tectonic processes (Kinny et al., 2005 and references therein). This craton-scale debate reflects a broader discussion about the nature and evolution of Earth's geodynamic regime(s) during the Archean and Proterozoic Eons, which remains a topic of significant debate (e.g., Arndt, 2013; Kamber, 2015; Bédard, 2018).

In the last 10 years, several important contributions to this research topic have assessed the temporal evolution of several geochemical and geological proxies, including the thermobarometric ratio recorded by metamorphic rocks (e.g., Brown, 2008; Brown and Johnson, 2018; Holder et al., 2019; Brown et al., 2020) and the bulk-rock composition of mafic and/or granitoid rocks (Dhuime et al., 2015; Condie, 2018; Moyen and Laurent, 2018; Smithies et al., 2018; Johnson et al., 2019). These records highlight evidence for a significant evolution on Earth between 3.5 and 2.2 Ga, which is often interpreted as reflecting the onset of plate tectonics (Cawood et al., 2018; Tang et al., 2018). Other authors point out that direct geological evidence for plate tectonics — such as the presence of ophiolites and blueschists — are almost exclusively concentrated in rocks younger than 1 Ga (Stern, 2008, 2020). Alternatively, zircon grains from Jack Hills record an emergence of peraluminous granitic rocks at 3.6 Ga, which could be the product of widespread subduction and the onset of plate tectonics (Ackerson et al., 2021).

By combining these important observations with more spatially focused projects aiming to constrain the petrogenesis of units within their geological context, it may be possible to establish with greater confidence the specific geodynamic processes that operated during the Archean and Proterozoic Eons, and how these processes evolved through time. Ultramafic–mafic rocks have the potential to provide particularly important insights due to their formation in a broad-range of geological environments. In

the LGC, these potential interpretations include: layered intrusions remnants (Bowes et al., 1964; Guice et al., 2018a, 2020); accreted oceanic crust (Park and Tarney, 1987); fragments of Archean mantle (Guice et al., 2020); sagducted remnants of one or more greenstone belt(s) (Johnson et al., 2016); and mafic dyke fragments (Mason and Brewer 2004). The historic limitation — when attempting to constrain which of these hypothesis is most likely for individual, or suites of, Archean–Paleoproterozoic ultramafic–mafic bodies — is that the primary stratigraphy is disrupted by deformation and the primary geochemistry affected by metamorphism (e.g., Guice et al., 2018a, 2018b).

In this study, we have combined detailed field observations with widely available petrographic and geochemical techniques to demonstrate that four apparently similar ultramafic–mafic bodies in the Lewisian Gneiss Complex of the Outer Hebrides likely represent multiple magmatic events. We have also deciphered broad geological environments for their formation and considered how they relate, petrogenetically and temporally, to other ultramafic–mafic rocks in the LGC and broader NAC (Section 6.4). This adds to a number of recent papers — focusing on ultramafic–mafic rocks — that have successfully utilized similar approaches to extract crucial information about the evolution of various Archean cratons (Szilas et al., 2014, 2015; Anhaeusser, 2015; Grosch and Slama, 2017; Guice et al., 2018a, 2018b, 2019; Pinheiro et al., 2021). Such first-order geological constraints are vitally important if we are to successfully apply modern, high-precision isotopic constraints (e.g., Sm-Nd; Re-Os) to ultramafic–mafic bodies and, ultimately, utilize their potential to provide crucial insights into the geodynamic processes responsible for the creation and destruction of Earth's lithosphere during the Archean and Proterozoic Eons.

7.0 CONCLUSIONS

1. This study identifies a previously unrecognized phase of ultramafic–mafic magmatism in the LGC: a suite of Archean cumulates represented by the Maaruig and Loch Mhorsgail bodies in the Outer Hebrides of Lewis and Harris. These occurrences are likely older than, or broadly coeval with, the

protoliths to the TTG gneiss that comprise the majority of the LGC (> 2.8 Ga). They are also geochemically distinct from anything currently identified in the mainland LGC's Central Region, potentially suggesting that the Outer Hebrides of Lewis and Harris (west of the OHFZ) was a distinct crustal block to that of the mainland LGC's Central Region in the late Mesoarchean.

2. A second group of ultramafic–mafic bodies — represented by the Coltraiseal Mor and Beinn a' Chuailean bodies — are likely dismembered Paleoproterozoic dykes that could be correlatives of the mainland Scourie dykes (extension-related, ca. 2.4 Ga ultramafic–mafic dykes). This supports recent U-Pb zircon geochronology (Davies and Heaman 2014), which assigned a 2.41 Ga crystallization age to a proposed Scourie Dykes in the Outer Hebrides (the Cleitichean Beag Dyke). It also suggests that the Outer Hebridean and mainland portions of the LGC were proximal to one another by the early Paleoproterozoic, placing an important constraint on the tectonic evolution of the LGC.

ACKNOWLEDGEMENTS

GLG would like to thank Tony Oldroyd for producing a suite of high quality polished thin sections and Ellis Krishan, who crushed and ground the samples to fine powders. GLG also thanks the Society of Economic Geologists (Graduate Fellowship Award) for providing a generous bursary in 2016 (when the lead author was a graduate student), which enabled some of the fieldwork conducted as part of this study. SRM thanks Christ's College for providing funding in 2019 to support fieldwork, Ben Akrill for assistance during fieldwork, Catriona Morrison and family for their hospitality during fieldwork at Maaruig, and the Mhorsgail Estate for providing assistance with land access at Mhorsgail.

TABLES

Table 1: Modal mineralogy for each sample assessed as part of this study. Abbreviations: Col. Mor = Coltraiseal Mor; BaC = Beinn a' Chuailean; ol = olivine; opx = orthopyroxene; cpx = clinopyroxene; amph = amphibole; ox = oxide phases; plag = plagioclase; phlo = phlogopite; Acc. = accessory phase.

Locality	Sample	Grid ref (NB)	ol	opx	cpx	amph	ox	plag	phlo	Rock name
Maaruig	Lw16_827	20398/06292	60	6	2.5	30	1.5			Metaperidotite
Maaruig	Lw16_828	20502/06187	40	22.5	1	35	1.5			Metapyroxenite
Maaruig	Lw16_903	20332/06278	79	11	1	7	2			Metaperidotite
Maaruig	Lw16_905	20023/06159	35	17	2	45	1			Metapyroxenite
Mhorsgail	Lw16_863	13415/22692	27	22	3	46	2			Metapyroxenite
Mhorsgail	Lw16_869	13409/22624	34	40		25	1		Acc.	Metapyroxenite
Mhorsgail	Lw16_871a	13516/22167	35	15		47	2.5		0.5	Metapyroxenite
Mhorsgail	Lw16_871b	13516/22167	68			30	2	Acc.	Acc.	Metaperidotite
Mhorsgail	Lw16_871c	13516/22167	50	5		43	2			Metaperidotite
Mhorsgail	Lw16_872	13726/21610	34	22		43	1		Acc.	Metapyroxenite
Col. Mor	Lw16_873	16498/22005	5	38	4	45	Acc.	6	2	Metagabbronorite
Col. Mor	Lw16_883	16546/22050	4	39	10	31	Acc	15	1	Metagabbronorite
Col. Mor	Lw16_884	16570/22091	5	38	12	30	1	12.5	1.5	Metagabbronorite
BaC	Lw16_899	19791/24719	15	40	20	15		8	2	Meta-ol gabbronorite
BaC	Lw16_900	19741/24717	3	25	25	19		8	20	Metagabbronorite

Table 2: Major and trace element analyses for each of the samples analyzed as part of this study.

Locality	Maaruig				Loch Mhorsgail					
Sample (Lw16_)	827	828	903	905	863	869	871A	871B	871C	872
Major elements (wt. %)										
SiO_2	42.76	43.77	42.95	42.34	44.33	46.41	40.14	44.10	43.55	46.57
TiO_2	0.19	0.22	0.15	0.29	0.14	0.15	0.17	0.20	0.17	0.20
Al_2O_3	4.35	3.79	2.31	4.91	1.99	2.39	2.54	3.38	2.84	3.40
Fe_2O_3	13.79	13.45	12.33	13.65	13.63	13.06	13.15	11.79	12.48	12.11
MnO	0.18	0.18	0.17	0.18	0.20	0.20	0.18	0.16	0.17	0.18
MgO	33.60	33.92	38.68	32.69	34.37	33.85	39.58	34.74	36.59	32.01
CaO	3.39	2.86	1.78	3.98	4.06	2.69	2.49	3.67	2.35	3.70
Na_2O	0.61	0.64	0.32	0.78	0.32	0.31	0.32	0.51	0.34	0.63
K_2O	0.16	0.19	0.12	0.22	0.06	0.05	0.14	0.29	0.30	0.08
P_2O_5	0.02	0.03	0.02	0.05	0.01	0.01	0.03	0.02	0.02	0.02
LOI	2.46	2.03	4.76	1.71	2.10	1.13	3.77	1.69	2.56	1.14
trace elements (ppm)										
V	93.1	83.5	62.6	104.1	95.4	88.7	76.4	90.1	80.3	96.8
Cr	6415	6362	7607	6461	5888	5536	8408	7437	7765	7404
Co	100.7	98.1	97.7	206.4	93.6	93.0	103.2	88.0	95.3	88.4
Ni	1927	1768	2092	1692	1570	1325	2141	1899	2005	1674
Cu	16.63	26.94	10.52	132.94	8.65	10.77	12.18	11.30	14.56	16.35
Zn	129.9	124.6	107.6	152.5	112.3	100.4	111.8	98.6	119.6	91.4
Ga	4.94	4.41	3.02	5.96	2.57	3.11	3.45	4.68	3.80	5.62
Rb	2.46	3.76	2.72	2.94	0.74	1.07	5.16	13.84	14.48	0.81
Sr	51.00	62.93	20.37	78.66	18.73	23.44	18.56	23.67	19.27	41.22
Y	4.46	4.61	2.94	7.04	2.57	2.74	3.21	4.57	2.26	4.38
Zr	13.74	16.91	4.56	20.45	8.08	3.61	1.71	6.56	2.46	13.24
Nb	1.94	1.51	0.92	2.57	0.71	0.40	0.45	0.88	1.00	0.90
Cs	n.d	0.07	0.04	0.03	n.d	0.03	0.15	0.40	0.30	n.d
Ba	37.17	39.03	11.22	20.70	2.46	2.05	16.58	37.96	59.12	4.00
La	2.51	4.38	2.00	6.61	1.10	1.83	2.79	3.05	2.40	3.02
Ce	5.43	8.84	4.42	13.50	2.35	4.48	6.06	6.76	5.31	7.81
Pr	0.69	0.98	0.53	1.54	0.28	0.54	0.72	0.77	0.53	0.91
Nd	3.10	4.08	2.24	6.35	1.40	2.24	2.89	3.26	1.93	3.72
Sm	0.74	0.84	0.50	1.36	0.39	0.49	0.59	0.75	0.38	0.86
Eu	0.23	0.24	0.13	0.35	0.10	0.15	0.14	0.19	0.12	0.22
Gd	0.67	0.78	0.44	1.20	0.41	0.40	0.48	0.69	0.37	0.72
Tb	0.13	0.14	0.08	0.21	0.07	0.07	0.09	0.12	0.06	0.12
Dy	0.74	0.77	0.47	1.20	0.47	0.43	0.54	0.71	0.38	0.74
Ho	0.15	0.15	0.10	0.23	0.10	0.09	0.11	0.15	0.08	0.14
Er	0.41	0.44	0.25	0.65	0.26	0.27	0.29	0.43	0.21	0.40
Tm	0.07	0.06	0.04	0.10	0.04	0.05	0.05	0.06	0.03	0.06
Yb	0.43	0.47	0.27	0.62	0.26	0.28	0.30	0.45	0.23	0.41
Lu	0.06	0.07	0.04	0.10	0.05	0.04	0.05	0.08	0.03	0.07
Hf	0.43	0.47	0.18	0.59	0.23	0.13	0.06	0.25	0.19	0.33
Ta	0.11	0.08	0.05	0.14	0.03	0.04	0.05	0.07	0.05	0.07
Pb	0.59	0.93	0.51	0.80	1.80	0.30	2.15	4.23	50.54	0.66
Th	3.06	1.98	1.29	1.95	2.28	0.91	0.82	0.94	0.92	1.09
U	0.09	0.17	0.10	0.31	0.05	0.08	0.12	0.12	0.09	0.11
Normalized trace element ratios										
$[La/Lu]_{ch}N$	4.13	6.33	4.78	6.98	2.39	4.83	6.06	4.10	8.27	4.56
$[La/Sm]_{ch}N$	2.11	3.27	2.49	3.04	1.74	2.33	2.98	2.54	3.90	2.20
$[Nb/La]_{pm}N$	0.76	0.34	0.45	0.38	0.63	0.21	0.16	0.28	0.41	0.29
$[Th/Yb]_{pm}N$	39.10	23.12	26.70	17.37	48.80	18.16	15.28	11.46	21.93	14.80
$[Ta/Yb]_{pm}N$	2.94	2.02	2.38	2.69	1.49	1.73	2.06	1.75	2.63	2.11

Table 2 (cont.):

Locality	Coltraiseal Mor			Beinn a' Chuailein	
Sample (Lw16_)	873	883	884	889	900
Major elements (wt. %)					
SiO_2	52.70	51.37	50.54	51.22	50.96
TiO_2	0.38	0.39	0.35	0.44	0.65
Al_2O_3	5.78	6.56	5.72	6.26	7.62
Fe_2O_3	10.20	11.76	12.29	11.91	12.76
MnO	0.18	0.19	0.19	0.19	0.19
MgO	20.29	21.94	23.55	21.85	18.96
CaO	8.67	6.00	5.78	6.25	6.35
Na_2O	0.93	0.88	0.71	0.95	1.39
K_2O	0.31	0.41	0.32	0.44	0.67
P_2O_5	0.02	0.04	0.03	0.05	0.08
LOI	0.00	1.12	0.00	0.00	0.00
trace elements (ppm)					
V	180.0	145.5	148.3	146.1	178.3
Cr	3725	3172	3373	3089	2641
Co	55.6	66.8	587.6	66.2	60.9
Ni	709	862	1087	850	543
Cu	28.83	26.79	648.88	39.91	41.48
Zn	77.6	95.0	94.4	100.0	94.2
Ga	9.04	7.57	7.49	8.99	9.47
Rb	10.61	13.11	8.51	12.97	15.02
Sr	78.52	104.23	84.72	91.12	91.03
Y	8.40	8.07	6.54	8.49	12.27
Zr	24.03	18.43	8.36	30.65	24.38
Nb	1.56	1.09	3.13	2.40	2.14
Cs	0.18	0.15	0.12	0.18	0.21
Ba	88.00	108.76	94.35	134.67	194.10
La	5.23	5.86	4.58	6.41	7.86
Ce	11.73	12.68	9.96	13.87	16.65
Pr	1.40	1.49	1.17	1.63	1.88
Nd	5.87	5.89	4.93	6.61	7.88
Sm	1.39	1.23	1.07	1.27	1.68
Eu	0.39	0.42	0.33	0.40	0.49
Gd	1.32	1.20	1.08	1.43	1.58
Tb	0.23	0.22	0.19	0.22	0.27
Dy	1.45	1.28	1.15	1.39	1.62
Ho	0.27	0.24	0.22	0.26	0.29
Er	0.82	0.75	0.59	0.73	0.82
Tm	0.13	0.11	0.10	0.11	0.14
Yb	0.79	0.74	0.63	0.75	0.89
Lu	0.11	0.11	0.09	0.12	0.13
Hf	0.75	0.64	0.31	0.90	0.89
Ta	0.11	0.13	0.19	0.16	0.19
Pb	2.01	2.31	1.39	4.04	3.63
Th	1.44	1.89	1.79	11.49	2.74
U	0.19	0.23	0.17	0.24	0.30
Normalized trace element ratios					
$[La/Lu]_{ch}N$	4.86	5.77	5.53	5.75	6.29
$[La/Sm]_{ch}N$	2.35	2.98	2.66	3.15	2.93
$[Nb/La]_{pm}N$	0.29	0.18	0.67	0.37	0.27
$[Th/Yb]_{pm}N$	10.13	14.16	15.66	85.42	17.02
$[Ta/Yb]_{pm}N$	1.66	2.03	3.58	2.49	2.48

REFERENCES

Ackerson, M.R., Trail, D., and Buettner, J., 2021, Emergence of peraluminous crustal magmas and implications for the early Earth: Geochemical Perspective Letters, v. 17, p. 50–54.

Andersen, T., Whitehouse, M.J., and Burke, E.A.J., 1997, Fluid inclusions in Scourian granulites from the Lewisian complex of NW Scotland: evidence for CO2-rich fluid in Late Archaean high-grade metamorphism: Lithos, v. 40, p. 93–104.

Anhaeusser, C.R., 2006, A reevaluation of Archean intracratonic terrane boundaries on the Kaapvaal Craton, South Africa: Collisional suture zones? Geological Society of America, Special Paper, v. 405, p. 193–210.

Anhaeusser, C.R., 2015, Metasomatized and hybrid rocks associated with a Palaeoarchaean layered ultramafic intrusion on the Johannesburg Dome, South Africa: Journal of African Earth Sciences, v. 102, p. 203–217, doi:10.1016/j.jafrearsci.2014.10.012.

Arndt, N.T., 2013, Formation and Evolution of the Continental Crust: Geochemical Perspectives, v. 2, p. 405–533, doi:10.7185/geochempersp.2.3.

Arndt, N., 1999, Why was flood volcanism on submerged continental platforms so common in the Precambrian? Precambrian Research, v. 97, p. 155–164.

Baba, S., 1998, Proterozoic anticlockwise P–T path of the Lewisian Complex of South Harris, Outer Hebrides, NW Scotland: Journal of Metamorphic Geology, v. 16, p. 819–841.

Baba, S., 1999, Sapphirine-bearing orthopyroxene-kyanite/sillimanite granulites from South Harris, NW Scotland: evidence for Proterozoic UHT metamorphism in the Lewisian: Contributions to Mineralogy and Petrology, v. 136, p. 33–47.

Barnicoat, A.C., 1983, Metamorphism of the Scourian Complex, NW Scotland: Journal of Metamorphic Geology, v. 1, p. 163–182.

944 Barooah, B.C., and Bowes, D.R., 2009, Multi-episodic modification of high-grade terrane near Scourie
945 and its significance in elucidating the history of the Lewisian Complex: Scottish Journal of
946 Geology, v. 45, p. 19–41, doi:10.1144/0036-9276/01-384.

947 Beach, A., 1974, Amphibolitization of Scourian granulites: Scottish Journal of Geology, v. 10, p. 35–
948 43.

949 Beach, A., 1973, The mineralogy of high temperature shear zones at Scourie, N.W. Scotland: Journal
950 of Petrology, v. 14, p. 231–248.

951 Beach, A., Coward, M.P., and Graham, R.H., 1974, An interpretation of the structural evolution of the
952 Laxford Front, north-west Scotland: Scottish Journal of Geology, v. 9, p. 297–308.

953 Bédard, J.H., 2013, How many arcs can dance on the head of a plume? A “comment” on: A critical
954 assessment of neoarchean “plume only” geodynamics: Evidence from the superior province, by
955 Derek Wyman, precambrian research, 2012: Precambrian Research, v. 229, p. 189–197,
956 doi:10.1016/j.precamres.2012.05.004.

957 Bédard, J.H., 2018, Stagnant lids and mantle overturns : Implications for Archaean tectonics ,
958 magmagenesis , crustal growth , mantle evolution , and the start of plate tectonics: Geoscience
959 Frontiers, v. 9, p. 19–49, doi:10.1016/j.gsf.2017.01.005.

960 Bowes, D.R., Park, R.G., and Wright, A.E., 1964, Layered intrusive rocks in the Lewisian of the North-
961 West Highlands of Scotland: Quarterly Journal of the Geological Society, v. 120, p. 153,
962 doi:10.1144/gsjgs.120.1.0153.

963 Bowes, D.R., Wright, A.E., and Park, R.G., 1966, Origin of Ultrabasic and Basic Masses in Lewisian:
964 Geological Magazine, v. 103, p. 280-, doi:10.1017/S0016756800053449.

965 Brown, M., 2008, Characteristic thermal regimes of plate tectonics and their metamorphic imprint
966 throughout Earth history: When did Earth first adopt a plate tectonic mode of behavior? The
967 Geological Society of America, Special Paper, v. 440, p. 97–113.

968 Brown, M., and Johnson, T., 2018, Secular change in metamorphism and the onset of global plate
969 tectonics: American Mineralogist, v. 103, p. 181–196, doi:10.2138/am-2018-6166.

970 Brown, M., Johnson, T., and Gardiner, N.J., 2020, Plate Tectonics and the Archean Earth: Annual
971 Review of Earth and Planetary Sciences, v. 48, p. 291–320.

972 Burton, K.W., Capmas, F., Birck, J.L., Allegre, C.J., and Cohen, A.S., 2000, Resolving crystallisation ages
973 of Archean mafic-ultramafic rocks using the Re-Os isotope system: Earth and Planetary Science
974 Letters, v. 179, p. 453–467.

975 Cann, J.R., 1970, Rb, Sr, Y, Zr and Nb in some ocean floor basaltic rocks: Earth and Planetary Science
976 Letters, v. 10, p. 7–11, doi:10.1016/0012-821X(70)90058-0.

977 Cartwright, I., Fitches, W.R., O'Hara, M.J., Barnicoat, A.C., and O'Hara, S., 1985, Archaean
978 supracrustal rocks from the Lewisian near Stoer, Sutherland: Scottish Journal of …, v. 21, p.
979 187–196, doi:10.1144/sjg21020187.

980 Cawood, P.A., Hawkesworth, C.J., Pisarevsky, S.A., Dhuime, B., Capitanio, F.A., and Nebel, O., 2018,
981 Geological archive of the onset of plate tectonics: Phil. Trans. R. Soc. Lond., v. 376.

982 Charlier, B., Vander Auwera, J., and Duchesne, J.C., 2005, Geochemistry of cumulates from the
983 Bjerkreim-Sokndal layered intrusion (S. Norway): Lithos, v. 83, p. 255–276,
984 doi:10.1016/j.lithos.2005.03.005.

985 Cheadle, M.J., McGeary, S., Warner, M.R., and Matthews, D.H., 1987, Extensional structures on the
986 western UK continental shelf: a review of evidence from deep seismic profiling: Geological
987 Society, London, Special Publications, v. 28, p. 445–465.

988 Cliff, R.A., Gray, C.M., and Huhma, H., 1983, A Sm-Nd isotopic study of the South Harris Igneous
989 Complex, the Outer Hebrides: Contributions to Mineralogy and Petrology, v. 82, p. 91–98,
990 doi:10.1007/BF00371178.

991 Cliff, R.A., and Rex, D.C., 1989, Short Paper: Evidence for a 'Grenville' event in the Lewisian of the
992 northern Outer Hebrides: Journal of the Geological Society, v. 146, p. 921–924.

993 Cliff, R.A., Rex, D.C., and Guise, P.G., 1998, Geochronological studies of Proterozoic crustal evolution
994 in the northern Outer Hebrides: Precambrian Research, v. 91, p. 401–418,
995 doi:http://dx.doi.org/10.1016/S0301-9268(98)00060-6.

996 Condie, K.C., 2018, A planet in transition: The onset of plate tectonics on Earth between 3 and 2 Ga?
997 Geoscience Frontiers, v. 9, p. 51–60, doi:10.1016/j.gsf.2016.09.001.

998 Corfu, F., 1998, U-Pb zircon systematics at Gruinard Bay, northwest Scotland : implications for the
999 early orogenic evolution of the Lewisian complex: Contributions to Mineralogy and Petrology,
1000 v. 133, p. 329–345.

1001 Corfu, F., Heaman, L.M., and Rogers, G., 1994, Polymetamorphic evolution of the Lewisian complex,
1002 NW Scotland, as recorded by U-Pb isotopic compositions of zircon, titanite and rutile:
1003 Contributions to Mineralogy and Petrology, v. 117, p. 215–228.

1004 Coward, M.P., Francis, P.W., Graham, R.H., Myers, J.S., and Watson, J., 1969, Remnants of an early
1005 metasedimentary assemblage in the Lewisian complex of the Outer Hebrides: Proceedings of
1006 the Geologists' Association, v. 80, p. 387–408.

1007 Crowley, Q.G., Key, R., and Noble, S.R., 2015, High-precision U–Pb dating of complex zircon from the
1008 Lewisian Gneiss Complex of Scotland using an incremental CA-ID-TIMS approach: Gondwana
1009 Research, v. 27, p. 1381–1391, doi:10.1016/j.gr.2014.04.001.

1010 Davies, F.B., 1974, A layered basic complex in the Lewisian, south of Loch Laxford, Sutherland:
1011 Journal of the Geological Society, v. 130, p. 279–284, doi:10.1144/gsjgs.130.3.0279.

1012 Davies, J.H.F.L., and Heaman, L.M., 2014, New U-Pb baddeleyite and zircon ages for the Scourie dyke
1013 swarm: A long-lived large igneous province with implications for the Paleoproterozoic evolution
1014 of NW Scotland: Precambrian Research, v. 249, p. 180–198,

1015 doi:10.1016/j.precamres.2014.05.007.

1016 Davies, F.B., Lisle, R.J., and Watson, J., 1975, The tectonic evolution of the Lewisian complex in
1017 northern Lewis, Outer Hebrides: Proceedings of the Geologists' Association, v. 86, p. 45–61.

1018 Dearnley, R., 1962, An Outline of the Lewisian Complex of the Outer Hebrides in Relation To That of
1019 the Scottish Mainland: Quarterly Journal of the Geological Society, v. 118, p. 143–176,
1020 doi:10.1144/gsjgs.118.1.0143.

1021 Dearnley, R., 1963, The Lewisian complex of South Harris With some observations on the
1022 metamorphosed basic intrusions of the Outer Hebrides , Scotland The paragneisses
1023 Paragneisses were first recognized and described from the Lewisian of South Harris: Quarterly
1024 Journal of the Geological Society, v. 119, p. 243–312.

1025 Dearnley, R., and Dunning, F., 1967, Metamorphosed and deformed pegmatites and basic dykes in
1026 the Lewisian complex of the Outer Hebrides and their geological significance: Quarterly Journal
1027 of the Geological Society, v. 123, p. 353–378.

1028 Debaille, V., Neill, C.O., Brandon, A.D., Haenecour, P., Yin, Q., Mattielli, N., and Treiman, A.H., 2013,
1029 Stagnant-lid tectonics in early Earth revealed by 142Nd in late Archean rocks: Earth and
1030 Planetary Science Letters, v. 373, p. 83–92, doi:10.1016/j.epsl.2013.04.016.

1031 Dhuime, B., Wuestefeld, A., and Hawkesworth, C.J., 2015, Emergence of modern continental crust
1032 about 3 billion years ago: Nature Geoscience, v. 8, p. 552–555, doi:10.1038/NGEO2466.

1033 Dilek, Y., and Polat, A., 2008, Suprasubduction zone ophiolites and Archean tectonics: Geology, v. 36,
1034 p. 431–432, doi:10.1016/0012.

1035 Evans, C.R., and Lambert, R.S.J., 1974, The Lewisian of Lochinver, Sutherland; the type area for the
1036 Inverian metamorphism: Journal of the Geological Society, v. 130, p. 125–150,
1037 doi:10.1144/gsjgs.130.2.0125.

1038 Faithfull, J.W., Dempster, T.J., MacDonald, J.M., and Reilly, M., 2018, Metasomatism and the
1039 crystallization of zircon megacrysts in Archaean peridotites from the Lewisian complex, NW
1040 Scotland: Contributions to Mineralogy and Petrology, v. 173, p. 99, doi:10.1007/s00410-018-
1041 1527-5.

1042 Feisel, Y., White, R.W., Palin, R.M., and Johnson, T.E., 2018, New constraints on granulite-facies
1043 metamorphism and melt pro- duction in the Lewisian Complex , northwest Scotland:

1044 Fettes, D.J., and Mendum, J.R., 1987, The evolution of the Lewisian complex in the Outer Hebrides:
1045 Geological Society Special Publications, v. 27, p. 27–44.

1046 Fettes, D.J., Mendum, J.R., Smith, D.I., and Watson, J. V, 1992, Geology of the Outer Hebrides.
1047 Memoir for 1: 100 000 (solid edition) geological sheets, Lewis and Harris, Uist and Barra
1048 (Scotland):

1049 Fischer, S., Prave, A.R., Johnson, T.E., Cawood, P.A., Hawkesworth, C.J., and Horstwood, M.S.A.,
1050 2021, Using zircon in mafic migmatites to disentangle complex high-grade gneiss terrains–
1051 Terrane spotting in the Lewisian complex, NW Scotland: Precambrian Research, v. 355, p.
1052 106074.

1053 Floyd, P.A., Winchester, J.A., and Park, R.G., 1989, Geochemistry and tectonic setting of Lewisian
1054 clastic metasediments from the Early Proterozoic Loch Maree Group of Gairloch, NW Scotland:
1055 Precambrian Research, v. 45, p. 203–214.

1056 Friend, C.R.L., and Kinny, P.D., 2001, A reappraisal of the Lewisian Gneiss Complex: geochronological
1057 evidence for its tectonic assembly from disparate terranes in the Proterozoic: Contributions to
1058 Mineralogy and Petrology, v. 142, p. 198–218, doi:10.1007/s004100100283.

1059 Furnes, H., de Wit, M., Staudigel, H., Rosing, M., and Muehlenbachs, K., 2007, A vestige of Earth's
1060 oldest ophiolite: Science, v. 315, p. 1704–1707, doi:10.1126/science.1139170.

1061 Godard, M., Jousselin, D., and Bodinier, J., 2000, Relationships between geochemistry and structure

1062 beneath a palaeo-spreading centre: a study of the mantle section in the Oman ophiolite: Earth
1063 and Planetary Science Letters, v. 180, p. 133–148.

1064 Godard, M., Lagabrielle, Y., Alard, O., and Harvey, J., 2008, Geochemistry of the highly depleted
1065 peridotites drilled at ODP Sites 1272 and 1274 (Fifteen-Twenty Fracture Zone, Mid-Atlantic
1066 Ridge): Implications for mantle dynamics beneath a slow spreading ridge: Earth and Planetary
1067 Science Letters, v. 267, p. 410–425, doi:10.1016/j.epsl.2007.11.058.

1068 Goodenough, K.M. et al., 2010, The Laxford Shear Zone: an end-Archaean terrane boundary?
1069 Geological Society, London, Special Publications, v. 335, p. 103–120, doi:10.1144/SP335.6.

1070 Goodenough, K.M., Crowley, Q.G., Krabbendam, M., and Parry, S.F., 2013, New u-pb age constraints
1071 for the Laxford Shear Zone, NW Scotland: Evidence fortectono-magmatic processes associated
1072 with the formation of a paleoproterozoic supercontinent: Precambrian Research, v. 232, p. 1–
1073 19, doi:10.1016/j.precamres.2013.05.006.

1074 Grosch, E.G., and Slama, J., 2017, Evidence for 3.3-billion-year-old oceanic crust in the Barberton
1075 greenstone belt, South Africa: Geology, v. 45, p. 1–4, doi:10.1130/G39035.1.

1076 Guice, G.L., 2019, Origin and geodynamic significance of ultramafic-mafic complexes in the North
1077 Atlantic and Kaapvaal Cratons: Cardiff University, http://orca.cf.ac.uk/123339/.

1078 Guice, G.L., McDonald, I., Hughes, H.S.R., and Anhaeusser, C.R., 2019, An evaluation of element
1079 mobility in the Modderfontein ultramafic complex, Johannesburg: Origin as an Archaean
1080 ophiolite fragment or greenstone belt remnant? Lithos, v. 332–333, p. 99–119,
1081 doi:10.1016/j.lithos.2019.02.013.

1082 Guice, G.L., McDonald, I., Hughes, H.S.R., MacDonald, J.M., Blenkinsop, T.G., Goodenough, K.M.,
1083 Faithfull, J.W., and Gooday, R.J., 2018a, Re-evaluating ambiguous age relationships in Archean
1084 cratons: Implications for the origin of ultramafic-mafic complexes in the Lewisian Gneiss
1085 Complex: Precambrian Research, v. 311, p. 136–156, doi:10.1016/j.precamres.2018.04.020.

1086 Guice, G.L., McDonald, I., Hughes, H.S.R., MacDonald, J.M., and Faithfull, J.W., 2020, Origin(s) and
1087 geodynamic significance of Archean ultramafic–mafic bodies in the mainland Lewisian Gneiss
1088 Complex, North Atlantic Craton: Journal of the Geological Society, v. 177, p. 700–717,
1089 doi:10.1144/jgs2020-013.

1090 Guice, G.L., McDonald, I., Hughes, H.S.R., Schlatter, D.M., Goodenough, K.M., Macdonald, J.M., and
1091 Faithfull, J.W., 2018b, Assessing the Validity of Negative High Field Strength-Element Anomalies
1092 as a Proxy for Archaean Subduction: Evidence from the Ben Strome Complex, NW Scotland:
1093 Geosciences, v. 8, p. 338, doi:10.3390/geosciences8090338.

1094 Hamilton, W.B., 2003, An alternative earth: GSA Today, v. 13, p. 4–12, doi:10.1130/1052-
1095 5173(2003)013<0004:AAE>2.0.CO;2.

1096 Heaman, L.M., and Tarney, J., 1989, U–Pb Baddeleyite ages for the Scourie Dyke Swarm, Scotland –
1097 evidence for 2 distinct intrusion events: Nature, v. 340, p. 705–708.

1098 Holder, R.M., Viete, D.R., Brown, M., and Johnson, T.E., 2019, Metamorphism and the evolution of
1099 plate tectonics: Nature, v. 572, p. 378–381, doi:10.1038/s41586-019-1462-2.

1100 Hollis, J.A., Harley, S.L., White, R.W., and Clarke, G.L., 2006, Preservation of evidence for prograde
1101 metamorphism in ultrahigh-temperature, high-pressure kyanite-bearing granulites, South
1102 Harris, Scotland: Journal of Metamorphic Geology, v. 24, p. 263–279, doi:10.1111/j.1525-
1103 1314.2006.00636.x.

1104 Huber, H., Koeberl, C., McDonald, I., and Reimold, W.U., 2001, Geochemistry and petrology of
1105 Witwatersrand and dwyka diamictites from south Africa: Search for an extraterrestrial
1106 component: Geochimica et Cosmochimica Acta, v. 65, p. 2007–2016, doi:10.1016/S0016-
1107 7037(01)00569-5.

1108 Hughes, H.S.R., McDonald, I., Goodenough, K.M., Ciborowski, T.J.R., Kerr, A.C., Davies, J.H.F.L., and
1109 Selby, D., 2014, Enriched lithospheric mantle keel below the Scottish margin of the North

1110 Atlantic Craton: Evidence from the Palaeoproterozoic Scourie Dyke Swarm and mantle
1111 xenoliths: Precambrian Research, v. 250, p. 97–126, doi:10.1016/j.precamres.2014.05.026.

1112 Imber, J., Holdsworth, R.E., Butler, C.A., and Lloyd, G.E., 1997, Fault-zone weakening processes along
1113 the reactivated Outer Hebrides Fault Zone: Journal of the Geological Society, v. 154, p. 105–
1114 109.

1115 Imber, J., Strachan, R.A., Holdsworth, R.E., and Butler, C.A., 2002, The initiations and early tectonic
1116 significance of the Outer Hebrides Fault Zone, Scotland: Geological Magazine, v. 139, p. 609–
1117 619, doi:10.1017/S0016756802006969.

1118 Jehu, T.J., and Craig, R.M., 1924, Geology of the Outer Hebrides. Part I.—The Barra Isles: Earth and
1119 Environmental Science Transactions of The Royal Society of Edinburgh, v. 53, p. 419–441.

1120 Jehu, T.J., and Craig, R.M., 1927, XX.—Geology of the Outer Hebrides. Part IV.—South Harris: Earth
1121 and Environmental Science Transactions of The Royal Society of Edinburgh, v. 55, p. 457–488.

1122 Jehu, T.J., and Craig, R.M., 1934, XXXIV.—Geology of the Outer Hebrides. Part V.—North Harris and
1123 Lewis: Earth and Environmental Science Transactions of The Royal Society of Edinburgh, v. 57,
1124 p. 839–874.

1125 Johnson, T.E., Brown, M., Goodenough, K.M., Clark, C., Kinny, P.D., and White, R.W., 2016,
1126 Subduction or sagduction ? Ambiguity in constraining the origin of ultramafic – mafic bodies in
1127 the Archean crust of NW Scotland: Precambrian Research, v. 283, p. 89–105,
1128 doi:10.1016/j.precamres.2016.07.013.

1129 Johnson, T.E., Fischer, S., White, R.W., Brown, M., and Rollinson, H.R., 2012, Archaean intracrustal
1130 differentiation from partial melting of metagabbro-field and geochemical evidence from the
1131 central region of the Lewisian complex, NW Scotland: Journal of Petrology, v. 53, p. 2115–2138,
1132 doi:10.1093/petrology/egs046.

1133 Johnson, T.E., Kirkland, C.L., Gardiner, N.J., Brown, M., Smithies, R.H., and Santosh, M., 2019, Secular

change in TTG compositions: Implications for the evolution of Archaean geodynamics: Earth and Planetary Science Letters, v. 505, p. 65–75, doi:10.1016/j.epsl.2018.10.022.

Kamber, B.S., 2015, The evolving nature of terrestrial crust from the Hadean, through the Archaean, into the Proterozoic: Precambrian Research, v. 258, p. 48–82, doi:10.1016/j.precamres.2014.12.007.

Kelly, N.M., Hinton, R.W., Harley, S.L., and Appleby, S.K., 2008, New SIMS U-Pb zircon ages from the Langavat Belt, South Harris, NW Scotland: Implications for the Lewisian terrane model: Journal of the Geological Society, v. 165, p. 967–981, doi:10.1144/0016-76492007-116.

Kinny, P.D., and Friend, C.R.L., 1997, U-Pb isotopic evidence for the accretion of different crustal blocks to form the Lewisian Complex of northwest Scotland: Contributions to Mineralogy and Petrology, v. 129, p. 326–340, doi:10.1007/s004100050340.

Kinny, P., Friend, C., and Love, G., 2005, Proposal for a terrane-based nomenclature for the Lewisian Gneiss Complex of NW Scotland: Journal of the Geological Society, v. 162, p. 175–186, doi:10.1144/0016-764903-149.

Kisters, A.F.M., and Szilas, K., 2012, Geology of an Archaean accretionary complex – The structural record of burial and return flow in the Tartoq Group of South West Greenland: Precambrian Research, v. 220–221, p. 107–122, doi:10.1016/j.precamres.2012.07.008.

Klemme, S., Prowatke, S., Hametner, K., and Gunther, D., 2005, Partitioning of trace elements between rutile and silicate melts: Implications for subduction zones: Geochimica et Cosmochimica Acta, v. 69, p. 2361–2371, doi:10.1016/j.gca.2004.11.015.

Kusky, T.M., Li, J., and Tucker, R.D., 2001, The Archean Dongwanzi Oceanic Crust and Mantle: Science, v. 292, p. 1142–1146.

Kusky, T.M., Zhi, X., Li, J., Xia, Q., Raharimahefa, T., and Huang, X., 2007, Chondritic osmium isotopic composition of Archean: Gondwana Research, v. 12, p. 67–76, doi:10.1016/j.gr.2006.10.023.

1158 Lahaye, Y., Arndt, N., Byerly, G., Chauvel, C., Fourcade, S., and Gruau, G., 1995, The influence of
1159 alteration on the trace-element and Nd isotopic compositions of komatiites: Chemical Geology,
1160 v. 126, p. 43–64.

1161 Lodders, K., 2003, Solar System Abundances and Condensation Temperatures of the Elements: The
1162 Astrophysical Journal, v. 591, p. 1220–1247, doi:10.1086/375492.

1163 Love, G.J., Friend, C.R.L., and Kinny, P.D., 2010, Palaeoproterozoic terrane assembly in the Lewisian
1164 Gneiss Complex on the Scottish mainland, south of Gruinard Bay: SHRIMP U-Pb zircon
1165 evidence: Precambrian Research, v. 183, p. 89–111, doi:10.1016/j.precamres.2010.07.014.

1166 Love, G.J., Kinny, P.D., and Friend, C.R.L., 2004, Timing of magmatism and metamorphism in the
1167 Gruinard Bay area of the Lewisian Gneiss Complex: Comparisons with the Assynt Terrane and
1168 implications for terrane accretion: Contributions to Mineralogy and Petrology, v. 146, p. 620–
1169 636, doi:10.1007/s00410-003-0519-1.

1170 Ma, Q., Xu, Y.G., Zheng, J.P., Sun, M., Griffin, W.L., Wei, Y., Ma, L., and Yu, X., 2016, High-Mg adakitic
1171 rocks and their complementary cumulates formed by crystal fractionation of hydrous mafic
1172 magmas in a continental crustal magma chamber: Lithos, v. 260, p. 211–224,
1173 doi:10.1016/j.lithos.2016.05.024.

1174 MacDonald, J.M., and Goodenough, K.M., 2013, The South Barra shear zone: A composite Inverian-
1175 Laxfordian shear zone and possible terrane boundary in the Lewisian Gneiss Complex of the Isle
1176 of Barra, NW Scotland: Scottish Journal of Geology, v. 49, p. 93–103, doi:10.1144/sjg2011-463.

1177 MacDonald, J.M., Goodenough, K.M., Wheeler, J., Crowley, Q., Harley, S.L., Mariani, E., and Tatham,
1178 D., 2015, Temperature-time evolution of the Assynt Terrane of the Lewisian Gneiss Complex of
1179 Northwest Scotland from zircon U-Pb dating and Ti thermometry: Precambrian Research, v.
1180 260, p. 55–75, doi:10.1016/j.precamres.2015.01.009.

1181 MacDonald, J.M., Wheeler, J., Harley, S.L., Mariani, E., Goodenough, K.M., Crowley, Q., and Tatham,

1182 D., 2013, Lattice distortion in a zircon population and its effects on trace element mobility and
1183 U-Th-Pb isotope systematics: Examples from the Lewisian Gneiss Complex, northwest Scotland:
1184 Contributions to Mineralogy and Petrology, v. 166, p. 21–41, doi:10.1007/s00410-013-0863-8.

1185 Mason, A.J., 2016, The Palaeoproterozoic anatomy of the Lewisian Complex, NW Scotland: evidence
1186 for two 'Laxfordian' tectonothermal cycles: Journal of the Geological Society , v. 173, p. 153–
1187 169, doi:10.1144/jgs2015-026.

1188 Mason, A.J., and Brewer, T.S., 2004, Mafic dyke remnants in the Lewisian Complex of the Outer
1189 Hebrides, NW scotland: A geochemical record of continental break-up and re-assembly:
1190 Precambrian Research, v. 133, p. 121–141, doi:10.1016/j.precamres.2004.04.001.

1191 Mason, A.J., Parrish, R.R., and Brewer, T.S., 2004a, U–Pb geochronology of Lewisian orthogneisses in
1192 the Outer Hebrides, Scotland: implications for the tectonic setting and correlation of the South
1193 Harris Complex: Journal of the Geological Society, v. 161, p. 45–54, doi:10.1144/0016-764902-
1194 140.

1195 Mason, A.J., Temperley, S., and Parrish, R.R., 2004b, New light on the construction, evolution and
1196 correlation of the Langavat Belt (Lewisian Complex), Outer Hebrides, Scotland: field,
1197 petrographic and geochronological evidence for an early Proterozoic imbricate zone: Journal of
1198 the Geological Society, v. 161, p. 837–848.

1199 McDonald, I., and Viljoen, K.S., 2006, Platinum-group element geochemistry of mantle eclogites: a
1200 reconnaissance study of xenoliths from the Orapa kimberlite, Botswana: Applied Earth Science,
1201 v. 115, p. 81–93, doi:10.1179/174327506X138904.

1202 McDonough, W.F., and Sun, S. s., 1995, The composition of the Earth: Chemical Geology, v. 120, p.
1203 223–253, doi:10.1016/0009-2541(94)00140-4.

1204 Moyen, J., and Laurent, O., 2018, Archaean tectonic systems : A view from igneous rocks: Lithos, v.
1205 302–303, p. 99–125, doi:10.1016/j.lithos.2017.11.038.

1206 Myers, J.S., and Lisle, R.J., 1971, Zones of abundant Scourie dyke fragments and their significance in
1207 the Lewisian Complex of Western Harris, Outer Hebrides: Proceedings of the Geologists'
1208 Association, v. 82, p. 365–377, doi:10.1016/S0016-7878(71)80015-9.

1209 O'Hara, M.J., 1961, Zoned ultrabasic and basic gneiss masses in the early lewisian metamorphic
1210 complex at scourie, Sutherland: Journal of Petrology, v. 2, p. 248–276,
1211 doi:10.1093/petrology/2.2.248.

1212 Ordóñez-calderón, J.C., Polat, A., Fryer, B.J., Appel, P.W.U., Gool, J.A.M. Van, Dilek, Y., and Gagnon,
1213 J.E., 2009, Geochemistry and geodynamic origin of the Mesoarchean Ujarassuit and Ivisaartoq
1214 greenstone belts , SW Greenland: Lithos, v. 113, p. 133–157, doi:10.1016/j.lithos.2008.11.005.

1215 Park, R.G., 2005, The Lewisian terrane model: a review: Scottish Journal of Geology, v. 41, p. 105–
1216 118, doi:10.1144/sjg41020105.

1217 Park, R.G., Stewart, A.D., and Wright, A.E., 2002, The Hebridean Terrane, *in* The Geology of
1218 Scotland,.

1219 Park, R.G., and Tarney, J., 1987, The Lewisian complex: a typical Precambrian high-grade terrain?
1220 Geological Society, London, Special Publications, v. 27, p. 13–25,
1221 doi:10.1144/gsl.sp.1987.027.01.03.

1222 Paulick, H., Bach, W., Godard, M., Hoog, J.C.M. De, Suhr, G., and Harvey, J., 2006, Geochemistry of
1223 abyssal peridotites (Mid-Atlantic Ridge , 15 ° 20 ′ N , ODP Leg 209): Implications for fluid / rock
1224 interaction in slow spreading environments: Chemical Geology, v. 234, p. 179–210,
1225 doi:10.1016/j.chemgeo.2006.04.011.

1226 Peach, B.N., Horne, J., Gunn, A.G., and Clough, C.T., 1907, The Geological Structure of the North-
1227 West Highlands, *in* Memoir of the Geological Survey of Great Britain,.

1228 Pinheiro, M.A.P., Guice, G.L., and Magalhães, J.R., 2021, Archean–Ediacaran evolution of the Campos
1229 Gerais Domain- a reworked margin of the São Francisco paleocontinent (Brazil): Constraints

1230 from metamafic–ultramafic rocks: Geoscience Frontiers, p. 101201,
1231 doi:https://doi.org/10.1016/j.gsf.2021.101201.

1232 Polat, A., Frei, R., Appel, P.W.U., Dilek, Y., Fryer, B., Ordóñez-Calderón, J.C., and Yang, Z., 2008, The
1233 origin and compositions of Mesoarchean oceanic crust: Evidence from the 3075 Ma Ivisaartoq
1234 greenstone belt, SW Greenland: Lithos, v. 100, p. 293–321, doi:10.1016/j.lithos.2007.06.021.

1235 Rollinson, H., and Gravestock, P., 2012, The trace element geochemistry of clinopyroxenes from
1236 pyroxenites in the Lewisian of NW Scotland: Insights into light rare earth element mobility
1237 during granulite facies metamorphism: Contributions to Mineralogy and Petrology, v. 163, p.
1238 319–335, doi:10.1007/s00410-011-0674-8.

1239 Rollinson, H.R., and Windley, B.F., 1980, An archaean granulite-grade tonalite-trondhjemite-granite
1240 suite from scourie, NW Scotland: Geochemistry and origin: Contributions to Mineralogy and
1241 Petrology, v. 72, p. 265–281, doi:10.1007/BF00376145.

1242 Sandeman, H.A., and Ryan, J.J., 2008, The Spi Lake Formation of the central Hearne domain, western
1243 Churchill Province, Canada: an axial intracratonic continental tholeiite trough above the
1244 cogenetic Kaminak dyke swarm: Canadian Journal of Earth Sciences, v. 45, p. 745–767.

1245 Schaen, A.J., Cottle, J.M., Singer, B.S., Brenhin Keller, C., Garibaldi, N., and Schoene, B., 2017,
1246 Complementary crystal accumulation and rhyolite melt segregation in a late Miocene Andean
1247 pluton: Geology, v. 45, p. 835–838, doi:10.1130/G39167.1.

1248 Shaw, R.A., Goodenough, K.M., Roberts, N.M.W., Horstwood, M.S.A., Chenery, S.R., and Gunn, A.G.,
1249 2016, Petrogenesis of rare-metal pegmatites in high-grade metamorphic terranes: A case study
1250 from the Lewisian Gneiss Complex of north-west Scotland: Precambrian Research, v. 281, p.
1251 338–362, doi:10.1016/j.precamres.2016.06.008.

1252 Sills, J.D., 1981, Geochemical studies of the Lewisian Complex of the western Assynt region, NW
1253 Scotland: University of Leicester.

1254 Sills, J.D., Savage, D., Watson, J. V., and Windley, B.F., 1982, Layered ultramafic-gabbro bodies in the
1255 Lewisian of northwest Scotland: geochemistry and petrogenesis: Earth and Planetary Science
1256 Letters, v. 58, p. 345–360, doi:10.1016/0012-821X(82)90085-1.

1257 Smithies, R.H., Ivanic, T.J., Lowrey, J.R., Morris, P.A., Barnes, S.J., Wyche, S., and Lu, Y., 2018, Two
1258 distinct origins for Archean greenstone belts: Earth and Planetary Science Letters, v. 487, p.
1259 106–116.

1260 Soldin, S.R., 1978, The tectonic evolution and geochemistry of the Lewisian Complex of North Harris:
1261 Imperial College of Science and Technology, University of London,
1262 doi:10.1017/CBO9781107415324.004.

1263 Stepanova, A., and Stepanov, V., 2010, Paleoproterozoic mafic dyke swarms of the Belomorian
1264 Province, eastern Fennoscandian Shield: Precambrian Research, v. 183, p. 602–616.

1265 Stern, R.J., 2005, Evidence from ophiolites, blueschists, and ultrahigh-pressure metamorphic
1266 terranes that the modern episode of subduction tectonics began in Neoproterozoic: Geology, v.
1267 33, p. 557–560.

1268 Stern, R.J., 2016, Is plate tectonics needed to evolve technological species on exoplanets?
1269 Geoscience Frontiers, v. 7, p. 573–580, doi:10.1016/j.gsf.2015.12.002.

1270 Stern, R.J., 2008, Modern-style plate tectonics began in Neoproterozoic time: An alternative
1271 interpretation of Earth's tectonic history: Special publication of the Geological Society of
1272 America, v. 440, p. 265–280.

1273 Stern, R.J., 2020, The Mesoproterozoic Single-Lid Tectonic Episode: Prelude to Modern Plate
1274 Tectonics: GSA Today, v. 30, p. 4–10, doi:https://doi.org/10.1130/GSATG480A.1.

1275 Sutton, J., and Watson, J.V., 1951, The pre-Torridonian metamorphic history of the Loch Torridon
1276 and Scourie areas in the northwest Highland, and its bearing on the chronological classification
1277 of the Lewisian: Quarterly Journal of the Geological Society, v. 106, p. 241–307.

1278 Szilas, K., Hinsberg, V.J. Van, Kisters, A.F.M., Hoffmann, J.E., Windley, B.F., Kokfelt, T.F., Scherstén, A.,
1279 Frei, R., Rosing, M.T., and Münker, C., 2013, Remnants of arc-related Mesoarchaean oceanic
1280 crust in the Tartoq Group of SW Greenland: Gondwana Research, v. 23, p. 436–451,
1281 doi:10.1016/j.gr.2011.11.006.

1282 Szilas, K., Van Hinsberg, V.J., Creaser, R.A., Kisters, A.F.M.M., Hinsberg, V. Van, and Kisters, A.F.M.M.,
1283 2014, The geochemical composition of serpentinites in the Mesoarchaean Tartoq Group, SW
1284 Greenland: Harzburgitic cumulates or melt-modified mantle? Lithos, v. 198–199, p. 103–116,
1285 doi:10.1016/j.lithos.2014.03.024.

1286 Szilas, K., Kelemen, P.B., and Bernstein, S., 2015, Peridotite enclaves hosted by Mesoarchaean TTG-
1287 suite orthogneisses in the Fiskefjord region of southern West Greenland: GeoResJ, v. 7, p. 22–
1288 34, doi:10.1016/j.grj.2015.03.003.

1289 Tang, M., Chen, K., and Rudnick, R.L., 2018, Archean upper crust transition from mafic to felsic marks
1290 the onset of plate tectonics: Science, v. 351, p. 372–375.

1291 Tarney, J., 1963, Assynt dykes and their metamorphism: Nature, v. 199, p. 672–674.

1292 Tarney, J., and Weaver, B.L., 1987, Mineralogy, petrology and geochemistry of the Scourie dykes:
1293 petrogenesis and crystallization processes in dykes intruded at depth: Geological Society,
1294 London, Special Publications, v. 27, p. 217–233, doi:10.1144/GSL.SP.1987.027.01.19.

1295 Taylor, R.J.M., Johnson, T.E., Clark, C., and Harrison, R.J., 2020, Persistence of melt-bearing Archean
1296 lower crust for > 200 m.y.— An example from the Lewisian Complex , northwest Scotland:
1297 Geology, v. 48, doi:10.1130/G46834.1/4906652/g46834.pdf.

1298 Teall, J.J.H., 1885, The metamorphosis of dolerite into hornblende-schist: Quarterly Journal of the
1299 Geological Society, v. 41.

1300 Watson, J., 1969, The Precambrian gneiss complex of Ness, Lewis, in relation to the effects of
1301 Laxfordian regeneration: Scottish Journal of Geology, v. 5, p. 269 LP – 285,

1302 doi:10.1144/sjg05030269.

1303 Weaver, B.L., and Tarney, J., 1981, The Scourie Dyke Suite: petrogenesis and geochemical nature of
1304 the Proterozoic sub-continental mantle: Contributions to Mineralogy and Petrology1, v. 78, p.
1305 175–188.

1306 Wheeler, J., Park, R.G., Rollinson, H.R., and Beach, A., 2010, The Lewisian Complex: insights into deep
1307 crustal evolution: Geological Society, London, Special Publications, v. 335, p. 51–79,
1308 doi:10.1144/SP335.4.

1309 Whitehouse, M.J., 1990, An early-Proterozoic age for the Ness anorthosite, Lewis, Outer Hebrides:
1310 Scottish Journal of Geology, v. 26, p. 131–136.

1311 Whitehouse, M.J., and Bridgwater, D., 2001, Geochronological constraints on Paleoproterozoic
1312 crustal evolution and regional correlations of the northern Outer Hebridean Lewisian complex,
1313 Scotland: Precambrian Research, v. 105, p. 227–245.

1314 Whitehouse, M.J., and Kemp, A.I.S., 2010, On the difficulty of assigning crustal residence, magmatic
1315 protolith and metamorphic ages to Lewisian granulites: constraints from combined in situ U-Pb
1316 and Lu-Hf isotopes: Geological Society, London, Special Publications, v. 335, p. 81–101,
1317 doi:10.1144/SP335.5.

1318 de Wit, M.J., Hart, R.A., and Hart, R.J., 1987, The Jamestown Ophiolite Complex, Barberton mountain
1319 belt: a section through 3.5 Ga oceanic crust: Journal of African Earth Sciences, v. 6, p. 681–730,
1320 doi:10.1016/0899-5362(87)90007-8.

1321 Yaxley, G.M., Crawford, A.J., and Green, D.H., 1991, Evidence for carbonatite metasomatism in spinel
1322 peridotite xenoliths from western Victoria , Australia: Earth and Planetary Science Letters, v.
1323 107, p. 305–317.

1324